Methane fluxes between terrestrial ecosystems and the atmosphere at northern high latitudes during the past century: A retrospective analysis with a process-based biogeochemistry model

Q. Zhuang,[1] J. M. Melillo,[1] D. W. Kicklighter,[1] R. G. Prinn,[2] A. D. McGuire,[3] P. A. Steudler,[1] B. S. Felzer,[1] and S. Hu[1]

[1]   We develop and use a new version of the Terrestrial Ecosystem Model (TEM) to study how rates of methane (CH_4) emissions and consumption in high-latitude soils of the Northern Hemisphere have changed over the past century in response to observed changes in the region's climate. We estimate that the net emissions of CH_4 (emissions minus consumption) from these soils have increased by an average 0.08 Tg CH_4 yr^{-1} during the twentieth century. Our estimate of the annual net emission rate at the end of the century for the region is 51 Tg CH_4 yr^{-1}. Russia, Canada, and Alaska are the major CH_4 regional sources to the atmosphere, responsible for 64%, 11%, and 7% of these net emissions, respectively. Our simulations indicate that large interannual variability in net CH_4 emissions occurred over the last century. Our analyses of the responses of net CH_4 emissions to the past climate change suggest that future global warming will increase net CH_4 emissions from the Pan-Arctic region. The higher net CH_4 emissions may increase atmospheric CH_4 concentrations to provide a major positive feedback to the climate system.   *INDEX TERMS:* 1610 Global Change: Atmosphere (0315, 0325); 1615 Global Change: Biogeochemical processes (4805); 1620 Global Change: Climate dynamics (3309); 1890 Hydrology: Wetlands; *KEYWORDS:* methane emissions, methane oxidation, permafrost

1.   Introduction

[2]   Soils have the capacity to both produce and consume methane (CH_4), a powerful greenhouse gas. A special group of soil microorganisms, the methanogens, is responsible for CH_4 production, while another group, the methanotrophs, is responsible for CH_4 consumption. Recent estimates put CH_4 emissions from the world's soils at between 150 and 250 Tg CH_4 yr^{-1} [*Prather et al.*, 2001], with a quarter to a third of the total emitted from the wet soils of high latitudes [*Walter et al.*, 2001a]. Estimates of CH_4 consumption by soil microbes are in the range of 10–30 Tg CH_4 yr^{-1} [*Prather et al.*, 2001], an order of magnitude lower than the emission estimates. Most of the CH_4 consumption occurs in the well-drained soils of temperate and tropical areas [*Ridgwell et al.*, 1999].

[3]   Terrestrial ecosystems north of 45°N have experienced earlier and more dramatic environmental changes from global warming compared with lower-latitude ecosystems, especially in the last decades of the twentieth century. These changes include higher mean annual air temperatures, increases in precipitation, and melting of permafrost [*Romanovsky et al.*, 2000; *Vitt et al.*, 2000; *Prather et al.*, 2001]. The warmer temperatures and the alterations of hydrology in the region have resulted in changes in the magnitude and timing of CH_4 emissions and consumption [e.g., *Friborg et al.*, 1997; *Whalen and Reeburgh*, 1992; *West and Schmidt*, 1998]. For example, larger CH_4 emissions have been observed earlier during the year that are associated with earlier spring thaws in sub-arctic mire ecosystems [e.g., *Friborg et al.*, 1997]. Larger CH_4 emissions have also been associated with increases in the thickness of the active layer in permafrost zones [*Whalen and Reeburgh*, 1992; *Moore et al.*, 1990; *Dise*, 1993].

[4]   Many of the regional and global estimates of CH_4 fluxes between the land and the atmosphere have been based on limited site measurements and simple extrapolation procedures [e.g., *Whalen and Reeburgh*, 1990b; *Whalen et al.*, 1991]. Recently, several large-spatial-scale models [e.g., *Cao et al.*, 1996; *Liu*, 1996; *Potter et al.*, 1996; *Prinn et al.*, 1999; *Ridgwell et al.*, 1999; *Walter and Heimann*, 2000; *Walter et al.*, 2001a, 2001b] have been

---

[1]Ecosystems Center, Marine Biological Laboratory, Woods Hole, Massachusetts, USA.

[2]Joint Program on the Science and Policy of Global Change, Massachusetts Institute of Technology, Cambridge, Massachusetts, USA.

[3]Alaska Cooperative Fish and Wildlife Research Unit, U.S. Geological Survey, University of Alaska Fairbanks, Fairbanks, Alaska, USA.

developed to estimate current and future methane exchanges between the land and the atmosphere. These models have incorporated many of the factors that control CH_4 fluxes and have led to major advances in our understanding of CH_4 fluxes to the atmosphere from northern ecosystems. However, the existing models have not considered the complex behavior of the freeze-thaw phenomena, i.e., the freezing of soil upward from the permafrost boundary as well as downward from the soil surface [see *Zhuang et al.*, 2001; *Goodrich*, 1978a, 1978b], in northern ecosystems when developing their estimates. We build on this solid foundation by explicitly considering the effects of permafrost freeze-thaw dynamics and vegetation carbon dynamics on the consumption and emissions of methane from soils.

[5] To estimate CH_4 fluxes between soils and the atmosphere, we have developed a new methane module and have coupled it to our process-based biogeochemistry model, the Terrestrial Ecosystem Model (TEM) [*Melillo et al.*, 1993; *Zhuang et al.*, 2003]. We use this model to estimate the ''net CH_4 emissions'' (i.e., emissions minus consumption) from the region north of 45°N during the 1990s. We then use the model to explore how these net CH_4 emissions have changed from 1900 to 2000.

2. Methods

2.1. Model Framework

[6] We have developed an hourly time step methane dynamics module (MDM) for TEM that explicitly considers the process of CH_4 production (methanogenesis) as well as CH_4 oxidation (methanotrophy) and the transport of the gas from the soil to the atmosphere. We have coupled the MDM with several existing TEM modules (Figure 1a): the core carbon and nitrogen dynamics module of TEM 5.0 (CNDM) [*Zhuang et al.*, 2003], the soil thermal module (STM) that includes permafrost dynamics [*Zhuang et al.*, 2001], and an improved and expanded hydrological module (HM) [*Zhuang et al.*, 2002] that simulates water movement across an atmosphere-vegetation-soil continuum. For northern ecosystems, the soil component of the HM considers moisture dynamics explicitly in moss, organic soil, and mineral soil layers [*Zhuang et al.*, 2002], and is designed to consider fluctuations in water table depth.

2.1.1. Methane Dynamics Module

[7] Fluxes of methane between soils and the atmosphere depend on the relative rates of methane production and oxidation within the soil profile and the transport of methane across the surface of soils. We assume that soils can be separated into an upper unsaturated zone and a lower saturated zone according to the water table depth. Methanotrophy (methane oxidation) occurs in the unsaturated zone and methanogenesis (methane production) occurs in the saturated zone. Because methanotrophy reduces soil methane concentrations in the unsaturated zone and methanogenesis increases soil methane concentrations in the saturated zone, the resulting concentration gradient causes methane to diffuse from the saturated zone into the unsaturated zone. If the rate of methanogenesis is larger than the rate of methanotrophy within the soil profile, such as occurs in wetland soils, methane will be emitted to the atmosphere
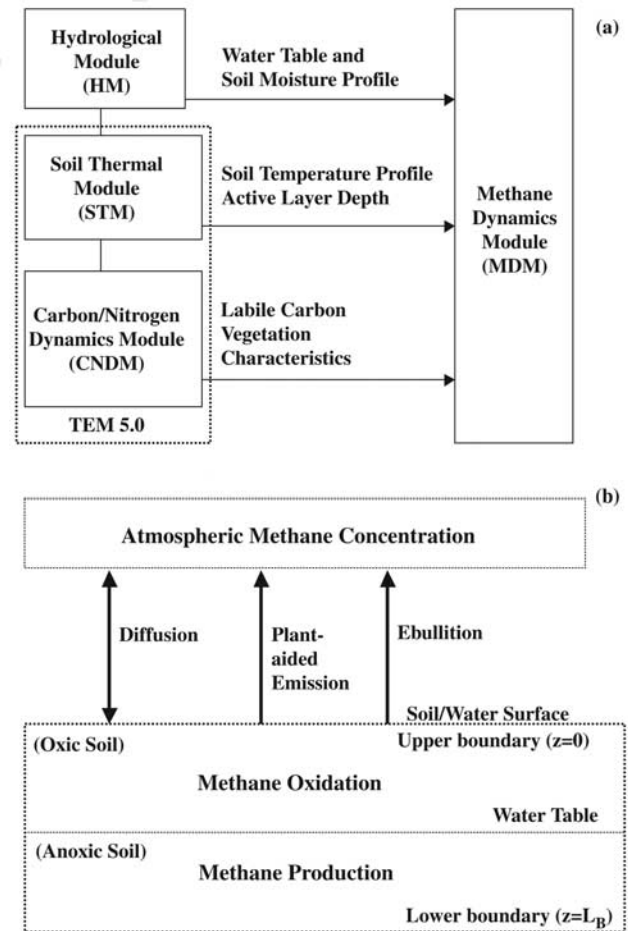

Figure 1. Schematic diagram of the new version of a biogeochemistry model (TEM) including (a) the overall model structure which features a soil thermal module (STM) [*Zhuang et al.*, 2001], an updated hydrologic module (HM) based on *Zhuang et al.* [2002], a carbon/nitrogen dynamics module (CNDM) from TEM 5.0 [*Zhuang et al.*, 2003], and a methane dynamics module (MDM); and (b) the more detailed structure of the MDM including the separation of soil into anaerobic and aerobic zones by water table position. The soil profile is divided into 1-cm layers that are referenced by their depth z from the upper boundary ($z = 0$) to a lower boundary (L_B, $z > 0$). The rates of CH_4 production and oxidation are determined with factors described in the text and Appendices A and B. The different transport pathways of CH_4 between soils and the atmosphere (diffusion, plant-aided transport, and ebullition) are described in the text and in Appendix C.

through diffusion. There are two other pathways in addition to diffusion that can be important for CH_4 transport to the atmosphere. Soil CH_4 can be transported from deep layers in sediments and soils through ''hollow tubes'' running from the roots through the stems to the leaves of some plants (plant-aided transport). If the water table is above the soil surface, methane can also move in bubbles through the

Table 1. Parameters of the Methane Dynamics Module for Major Ecosystem Types in the Northern High Latitudes[a]

	Alpine Tundra/Polar Desert		Moist/Wet Tundra		Boreal Forest		
	Wetland (Toolik-D)[b]	Upland (Tundra-NS)	Wetland (Toolik-W)	Upland (Tundra-UI)	Wetland (SSA-FEN)	Upland (B-F)	Unit
L_{MAXB}	100	100	100	100	110	100	cm
			Methanogenesis				
M_{G0}	0.45	0.45	1.0	0.45	1.3	0.8	μmol L^{-1} h^{-1}
NPP$_{MAX}$	100	100	150	100	250	250	gC m^{-2} month^{-1}
P_{Q10}	3.5	3.5	4.0	3.5	4.5	7.5	–
T_{PR}	−3.0	8.0	−5.5	8.0	10.0	7.0	°C
			Methanotrophy				
O_{MAX}	35	1.0	30	2.0	15	1.0	μmol L^{-1} h^{-1}
K_{CH4}	5.0	10.0	5.0	5.0	5.0	15	μmol L^{-1}
O_{Q10}	3.5	0.8	2.2	1.1	1.9	1.5	—
T_{OR}	−3.0	5.0	−5.5	5.5	10.0	5.4	°C
M_{VMAX}	1.0	0.9	1.0	0.7	1.0	1.0	% volume
M_{VMIN}	0.0	0.0	0.0	0.0	0.0	0.2	% volume
M_{VOPT}	0.5	0.4	0.5	0.3	0.5	0.6	% volume

[a]See text or notation section for the definition of variables.
[b]Names in parentheses represent sites used to calibrate the methane dynamics module; see Table 2.

overlying water and escape to the atmosphere. This transport process is known as ebullition.

[8] If the rate of methanotrophy is greater than the rate of methanogenesis within the soil profile, then most, if not all, of the methane produced in the saturated zone will be oxidized in the unsaturated zone and little or no CH$_4$ will be emitted from soils. Indeed, if the rate of methanogenesis is negligible, methanotrophy may cause a concentration gradient to develop that causes methane to diffuse from the atmosphere into the soil, such as occurs in well-drained upland soils. In this situation, soils are said to "consume" atmospheric methane.

[9] To simulate methane dynamics within the soil, we divide the soil column into a layered system with 1-cm increments from an upper boundary (i.e., the soil surface or water surface if the water table is above the soil surface) to a lower boundary (L_B), which represents the depth of microbial activity (Figure 1b). The L_B depends on active layer (i.e., unfrozen soil) depth as simulated by the soil thermal module. If the active layer depth is deeper than the maximum depth of microbial activity prescribed for an ecosystem (L_{MAXB}; see Table 1), the L_B is equal to L_{MAXB}; otherwise the L_B is equal to the active layer depth.

[10] Within each soil layer, changes in CH$_4$ concentration are governed by the following equation:

$$\frac{\partial C_M(z,t)}{\partial t} = M_P(z,t) - M_O(z,t) - \frac{\partial F_D(z,t)}{\partial z} - R_P(z,t) - R_E(z,t),$$
(1)

where $C_M(z, t)$ is the soil CH$_4$ concentration in μmol L^{-1} at depth z (centimeters) and time t (time step = 1 hour), $M_P(z, t)$ is the CH$_4$ production rate, $M_O(z, t)$ is the CH$_4$ oxidation rate, $R_P(z, t)$ is the plant-aided CH$_4$ emissions rate, and $R_E(z, t)$ is the ebullitive CH$_4$ emissions rate. The term, $\frac{\partial F_D(z,t)}{\partial z}$, the flux divergence, represents the net change in methane concentration resulting from the diffusion of methane into soil layer z from the surrounding soil layers or the atmosphere (if $z = 0$) and the diffusion of methane out of soil layer

z into the other soil layers or the atmosphere (if $z = 0$). The rates of diffusion and the emissions calculated for each soil layer within the soil profile are then used to determine the CH$_4$ flux at the soil or water surface. The CH$_4$ flux between the atmosphere and the soil ($F_{CH4}(t)$) is the total of the fluxes at the soil/water-atmosphere boundary via the different transport pathways,

$$F_{CH4}(t) = F_D(z = 0, t) + F_P(t) + F_E(t),$$
(2)

where $F_D(z = 0, t)$ is the diffusive flux of CH$_4$ between the atmosphere and the soil surface, $F_P(t)$ is the sum of all the plant-aided CH$_4$ emissions, and $F_E(t)$ is the sum of all the ebullitive CH$_4$ emissions. By numerically solving equation (1) for all the soil layers simultaneously, we obtain $F_D(z = 0, t)$ which will be positive if methane diffuses from the soil out to the atmosphere and will be negative if methane diffuses from the atmosphere into the soil. We determine $F_P(t)$ by integrating $R_P(z, t)$ for all soil layers between the soil surface and the rooting depth. Similarly, $F_E(t)$ is obtained by integrating $R_E(z, t)$ over all soil layers in the saturated zone if the water table is at or above the soil surface. Otherwise, the $F_E(t)$ term will equal 0.0. Emissions of CH$_4$ from soils occur when $F_{CH4}(t)$ is positive and CH$_4$ consumption by soils occurs when $F_{CH4}(t)$ is negative.

[11] As both biological activity and soil transport properties influence our estimates of CH$_4$ fluxes at the soil/water surface, we describe below how we obtain the terms in equation (1) in more detail.

2.1.1.1. Methane Production

[12] Methane production is modeled as an anaerobic process that occurs in the saturated zone of the soil profile. We estimate hourly methanogenesis ($M_P(z, t)$) within each 1-cm layer of the soil profile as follows:

$$M_P(z,t) = M_{G0} f(S_{OM}(z,t)) f(M_{ST}(z,t)) f(pH(z,t)) f(R_X(z,t)),$$
(3)

where M_{G0} is the ecosystem-specific maximum potential production rate (Table 1); $f(S_{OM}(z, t))$ is a multiplier that enhances methanogenesis with increasing methanogenic

substrate availability, which is a function of net primary production of the overlying vegetation; $f(M_{ST}(z, t))$ is a multiplier that enhances methanogenesis with increasing soil temperatures using a Q_{10} function [*Walter and Heimann*, 2000] with Q_{10} coefficients (P_{Q10}) and reference temperatures (T_{PR}) that vary across ecosystems (Table 1); $f(pH(t))$ is a multiplier that diminishes methanogenesis if the soil-water pH is not optimal (i.e., pH = 7.5) as described by *Cao et al.* [1996]; and $f(R_X(z, t))$ is a multiplier that describes the effects of the availability of electron acceptors which is related to redox potential on methanogenesis. To simulate $f(R_X(z, t))$, we use the relationships of *Zhang et al.* [2002] and *Fiedler and Sommer* [2000] where $f(R_X(z, t))$ diminishes methanogenesis linearly if redox potential is greater than -200 mV; otherwise, $f(R_X(z, t))$ is equal to 1.0. With the exception of $f(S_{OM}(z, t))$ which is described in section 2.1.4, the components of equation (3) are described in more detail in Appendix A.

2.1.1.2. Methane Oxidation

[13] Methane oxidation is modeled as an aerobic process that occurs in the unsaturated zone of the soil profile. We estimate hourly methanotrophy ($M_O(z, t)$) within each 1-cm layer of the soil profile as follows:

$$M_O(z,t) = O_{MAX} f(C_M(z,t)) f(T_{SOIL}(z,t)) f(E_{SM}(z,t)) f(R_{OX}(z,t)),$$

$$\text{(4)}$$

where O_{MAX} is the ecosystem-specific maximum oxidation coefficient (Table 1) that typically ranges between 0.3 and 360 μmol L^{-1} h^{-1} [*Segers*, 1998]; $f(C_M(z, t))$ is a multiplier that enhances methanotrophy with increasing soil methane concentrations using a Michaelis-Menten function with a half-saturation constant (K_{CH4}) that varies across ecosystems (Table 1); $f(T_{SOIL}(z, t))$ is a multiplier that enhances methanotrophy with increasing soil temperatures using a Q_{10} function [*Walter and Heimann*, 2000] with Q_{10} coefficients (O_{Q10}) and reference temperatures (T_{OR}) that vary across ecosystems (Table 1); $f(E_{SM}(z, t))$ is a multiplier that diminishes methanotrophy if the soil moisture is not at an optimum level (M_{vopt}); and $f(R_{OX}(z, t))$ is a multiplier that enhances methanotrophy as redox potentials increase linearly from -200 mV to 200 mV [*Zhang et al.*, 2002]. As redox potentials become greater than 200 mV, $f(R_{OX}(z, t))$ is set equal to 1.0. Methanotrophy is also assumed to cease if soil moistures reach a critical minimum (M_{vmin}) or maximum (M_{vmax}) soil moisture. These critical soil moistures along with the optimum soil moisture (M_{vopt}) are assumed to vary among ecosystems (Table 1). The components of equation (4) are described in more detail in Appendix B.

[14] The inputs to equations (3) and (4) are either prescribed for a site or provided by the other modules of the coupled model. Net primary production (NPP) is estimated by the CNDM. Soil temperatures are provided by the STM. Soil-water pH is prescribed for a site. Redox potential is calculated based on root distribution, the fraction of water-filled pore space, and the position of the water table [*Zhang et al.*, 2002; *Segers and Kengen*, 1998]. Root distribution is prescribed for a site based on ecosystem type. The fraction

of water-filled pore space, the position of the water table, and soil moisture are provided by the HM.

2.1.1.3. Methane Transport

[15] In the model, we consider three pathways by which CH$_4$ can be transported from the site of production in wetlands to the atmosphere: (1) diffusion through the soil profile ($F_D(z, t)$); (2) plant-aided transport ($R_P(z, t)$); and (3) ebullition ($R_E(z, t)$). In upland soils, we assume that diffusion of atmospheric methane into soils is the sole method of moving methane through the soil. We assume that soil diffusion follows Fick's law with a diffusion coefficient that varies with soil texture [*Walter et al.*, 2001a] and moisture status (i.e., saturated or unsaturated) of the soil layers [*Walter and Heimann*, 2000]. Plant-aided transport depends on vegetation type, plant density, the distribution of roots in the soil, and soil CH$_4$ concentrations [*Walter and Heimann*, 2000]. Ebullition occurs in saturated soil layers where the CH$_4$ concentration is greater than 500 μmol L^{-1} to allow bubbles to be formed [*Walter and Heimann*, 2000].

[16] The amount and timing of CH$_4$ emissions depend on the pathway used to transport methane to the atmosphere. Diffusion is relatively slow such that CH$_4$ produced in the lower saturated zone may be oxidized in the unsaturated zone before it can reach the atmosphere. In contrast, methane emissions from plant-aided transport or ebullitions, if the water table is at or above the soil surface, may reach the atmosphere from anywhere in the soil profile in a single hourly time step. However, if the water table is below the soil surface, bubbles formed in the saturated zone will contribute methane to the soil layer just above the water table. This methane will then continue to diffuse upward in the unsaturated zone where it may also be oxidized before reaching the atmosphere. Similar to *Walter and Heimann* [2000], we also assume that a portion of the methane transported by plants will be oxidized before the gas reaches the atmosphere. However, we assume that only 40 percent of the methane is oxidized as compared to the 50 percent assumed by *Walter and Heimann* [2000]. We describe how we modeled each of these transport pathways in more detail in Appendix C.

2.1.2. Soil Thermal Module

[17] The soil thermal module (STM) [*Zhuang et al.*, 2001, 2002, 2003] is used to estimate the active layer depth (i.e., the depth of unfrozen soil that varies seasonally) and soil temperatures at specified depths within the soil profile based on monthly or daily air temperatures and precipitation. In the module, the vertical profile is divided into six thermal layers: snowpack, moss (or litter), upper organic soil, lower organic soil, upper mineral soil, and lower mineral soil. Each of these thermal layers is characterized with a distinct soil thermal conductivity and heat capacity. The module considers two freezing fronts: (1) a front where soil freezes upward from the permafrost boundary and (2) a front where soil freezes downward from the ground surface. For the snowpack layer, a snow classification system [*Liston and Pielke*, 2000] has been implemented to better characterize the effect of seasonal changes in snow density and thermal conductivity within various ecosystems on the soil thermal regime at a large spatial scale. The soil thermal module has been designed to run at a flexible time step (e.g., 0.5 hour,

0.5 day) and several depth steps (e.g., 2 cm, 5 cm). The module has been calibrated and validated for major biomes in the Northern Hemisphere [*Zhuang et al.*, 2001, 2002] and the globe [*Zhuang et al.*, 2003].

[18] In this study, the methane dynamics module (MDM) requires the input of soil temperatures at each 1 cm depth of the soil layer in addition to the active layer depth. Therefore we use the STM to simulate the soil temperatures for a limited number of depths within the organic and mineral soil layers due to computational time constraints. The daily soil temperatures at each 1 cm depth are then obtained through linear interpolation of the daily soil temperatures estimated at the limited number of depths. When determining hourly CH_4 fluxes with the MDM, soil temperatures and the active layer depth are assumed to remain constant throughout the day.

2.1.3. Hydrological Module

[19] In this study, the methane module requires soil moisture estimates for each 1 cm soil layer within the profile and the estimated depth of the water table in wetland soils. We use an updated version of the hydrological module (HM) [*Zhuang et al.*, 2002] to provide these estimates. Module improvements include (1) the consideration of surface runoff when determining infiltration rates from rain throughfall and snowmelt, (2) the inclusion of the effects of temperature and vapor pressure deficit on canopy water conductance when estimating evapotranspiration based on *Waring and Running* [1998] and *Thornton* [2000], (3) a more detailed representation of water storage and fluxes within the soil profile of upland soils based on the use of the Richards equation in the unsaturated zone [*Hillel*, 1980], and (4) the development of daily estimates of soil moistures and water fluxes within the soil profile instead of monthly estimates. As the original version of the HM is designed to simulate water dynamics only in upland soils, algorithms have also been added to simulate water dynamics in wetland soils.

[20] For wetlands, the soil profile is divided into two zones based on the water table depth: (1) an oxygenated, unsaturated zone and (2) an anoxic, saturated zone. The soil water content and the water table depth in these wetland soils are determined using a water-balance approach that considers precipitation, runoff, drainage, snowmelt, snow sublimation, and evapotranspiration. We assume that wetland soils are always saturated below 30 cm, which represents the maximum water table depth [*Granberg et al.*, 1999]. Daily soil moisture at each 1 cm depth above the water table is modeled with a quadratic function and increases from the soil surface to the position of the water table [*Granberg et al.*, 1999]. Infiltration, runoff, snowmelt, snow sublimation, and evapotranspiration are simulated in wetlands using the same algorithms as for uplands. Drainage from wetlands is assumed to vary with soil texture, but does not exceed 20 mm d^{-1}. The modifications to the HM and the new wetland algorithms are described in more detail in Appendix D. When estimating hourly CH_4 fluxes with the MDM, soil moistures and the water table depth are assumed to remain constant throughout the day.

2.1.4. Carbon/Nitrogen Dynamics Module

[21] We assume that the production of root exudates during the growing season enhances methanogenesis by increasing the availability of organic carbon substrate. To capture the effect of the spatial and temporal variations in root exudates on methanogenesis, we use monthly net primary productivity (NPP) estimates from the carbon/nitrogen dynamics module (CNDM) of the Terrestrial Ecosystem Model (TEM) [*Zhuang et al.*, 2003]. The NPP estimates are used as an indicator for the seasonal and interannual variations in methanogenic substrate as follows:

$$f(S_{OM}(z,t)) = \left(1 + \frac{NPP(mon)}{NPP_{MAX}}\right) f(C_{DIS}(z)), \qquad (5)$$

where NPP(mon) is monthly net primary productivity (g C m^{-2} month^{-1}); NPP$_{MAX}$ represents the maximum monthly NPP expected for a particular vegetation type (Table 1); $f(C_{DIS}(z))$ is a multiplier that describes the relative availability of organic carbon substrate at depth z (centimeters) in the soil profile; and t represents time (hour). While organic substrates associated with fine root mortality are assumed to be available throughout the year, the ratio of NPP(mon) to NPP$_{MAX}$ is used to represent the additional availability of root exudates during the growing season (i.e., NPP greater than 0.0). Hence the first term on the right-hand side of equation (5) is assumed to equal 1.0 during the dormant season. We assume the simulated monthly NPP remains constant throughout the month. As a result of root mortality, we assume that $f(C_{DIS}(z))$ is equal to 1.0 throughout the rooting zone (i.e., z is above the rooting depth). If z is below the rooting depth, the effect of $f(C_{DIS}(z))$ is assumed to decrease exponentially with depth [*Walter and Heimann*, 2000] as follows:

$$f(C_{DIS}(z)) = e^{\frac{-(z-R_D)}{10.0}}, \qquad (6)$$

where R_D is the rooting depth (centimeters) as determined by the soil texture and the vegetation type [*Vörösmarty et al.*, 1989] found at the site.

2.2. Methane Dynamics Module Parameterization

[22] We parameterize the methane dynamics module (MDM) using measurements of CH_4 fluxes and key soil and climate factors made at six field sites in North America between 53°N and 68.5°N (Table 2). For wetland ecosystems, we parameterize the MDM by minimizing the differences between observed fluxes and simulated fluxes at the Toolik-D, Toolik-W, and SSA-FEN field sites. For each site, we start the parameterization procedure with an initial set of parameter values determined by a review of the literature. Each individual parameter has been adjusted to be within a range of values provided from the literature review until the root-mean-square error (RMSE) between the daily simulated and observed CH_4 fluxes is minimized. This procedure is conducted sequentially for all parameters with the result that RMSE for the Toolik-D, Toolik-W, and SSA-FEN parameterizations are 20, 52, and 42 mg CH_4 m^{-2} d^{-1}, respectively.

[23] Unlike the wetland sites, we do not have a daily time series of CH_4 flux data for the other three upland sites (B-F, Tundra-NS, and Tundra-UI). Therefore we parameterize the MDM for upland ecosystems such that the difference

Table 2. Site Descriptions Including Soil Characteristics, Driving Data, and Observational Data Used to Parameterize and Test the Model

Site Name	Location (Lon./Lat.)	Elevation, m	Vegetation	Soil and Climate Characteristics	Driving Climate Data	Observed Data	Sources and Comments
				Calibration Sites for Tundra Ecosystems			
Moist tundra on Unalaska Island (Tundra-UI)	167°W/53°N	-	wet tundra	air temperatures ranged from 5 to 8°C; soil pH is 5.7	climate data from Shemya USAF (lat. 52°43′N, lon.174°06′W)[a]	static chamber measured CH$_4$ uptake	*Whalen and Reeburgh* [1990a]; http://www.wrcc.dri.edu see http://ecosystems. mbl.edu/ARC and http://www.wrcc.dri.edu
Tundra at Toolik Station of Alaska (Toolik-D)	149° 36′W /68°38′N	760	tussock tundra	continuous permafrost, short cool summers, long cold winters; the soils unevenly covered with an organic mat 0–30 cm thick, underlain by a silty mineral soil. The maximum depth of thaw is 30–50 cm, soil pH is 5.0	air temperatures and precipitation (1991–1996) from the site, winter precipitation use 30-year average values of daily data at arctic village, Alaska station (lat. 68°08′N, lon. 145°32′W)	soil temperatures at depths 10, 20, and 50 cm, CH$_4$ fluxes of 1992 and 1993	*King et al.* [1998]; also see http://www-nsidc. colorado.edu/data/ arcss013.html
Tundra at Toolik Station of Alaska (Toolik-W)	same as above	760	wet tussock tundra	vegetation is wet tundra, soil pH is 5.0	same as above	soil temperatures at depths 3, 5, 7, 9, and 11 cm, CH$_4$ fluxes from 1994 and 1995 at the ARCSS-LAII site	
Tundra at north slope of Alaska (Tundra-NS)	-	-	sedge, moss tussock tundra	predominately saturated soils, continuous permafrost, thick peats	climate data from NOAA records for Fairbanks International Airport from 1986 to 1991[b]	static chamber CH$_4$ uptake	*King et al.* [1989]
				Calibration Sites for Boreal Forest Ecosystems			
Boreal forest at Bonanza Creek of Alaska (B-F)	148°15′W/64°41′N	133	black spruce, feather moss	Pergelic Cryaquepts, parent material is Alluvium, forest floor depth is 20 cm, intermittent permafrost. The active layer thickness is highly variable. Some years the frozen layer persists at a depth of 140 cm. Soil pH is 5.4	climate data from NOAA records for Fairbanks International Airport, 6 km south of study site, from 1986 to 1991	CH$_4$ fluxes from late May to September of 1990	*Whalen et al.* [1991]; see http://www.lter. uaf.edu/
Fen at southern study area of BOREAS (SSA-FEN)	105°57′W/53°57′N	524.7	complex fen with buckbean, sedges, birch, and willow	depth of peat is 1–3 m; high temperature (>20°C) and vapor pressure deficit (>1.5 kPa); soil pH is 7.1	daily temperature and precipitation are from the Canadian AES station-Nipawin station from 1994–1996; vapor pressure from the CRU data for the grid cell[c]	soil temperatures at 10 and 20 cm depth, daily evapo-transpiration and eddy covariance measurements of CH$_4$ fluxes for May to October of 1994 and 1995	*Sellers et al.* [1997]; *Newcomer et al.* [2000]; *Stryker et al.* [1996, 1997]
				Test Sites			
Tundra at Fairbanks of Alaska (Tundra-F)	147°51′W/64°52′N	158.5	tussock tundra, dominated by Eriophorum	poorly drained soil, underlain by permafrost; typical interior Alaska climate, little standing water, soils are saturated during freeze-up; soil pH is 5.4	climate data from NOAA records for Fairbanks International Airport, 6 km south of study site, from 1987 to 1990	three sites of CH$_4$ emissions observed using chamber techniques from 1987 to 1990	see *Whalen and Reeburgh* [1992]; *Ojima et al.* [2000]; http://www.nrel. colostate.edu/ projects/tragnet

Table 2. (continued)

Site Name	Location (Lon./Lat.)	Elevation, m	Vegetation	Soil and Climate Characteristics	Driving Climate Data	Observed Data	Sources and Comments
Fen at northern study area of BOREAS (NSA-FEN)	98°25′W/55°55′N	218	fen complex including sedge (Carex spp.), moss, moat, and shrubs	shrub-dominated hummock-hollow; permafrost peat plateau; soil pH ranges from 3.8 to 7.2.	daily temperature and precipitation from Manitoba station of Canadian AES from 1994 to 1996; vapor pressure data from CRU data sets for the grid cell	soil temperatures at depths 5, 10, 20, 50, and 100 cm; water table depth (1994) and chamber measurements of CH$_4$ fluxes of May–September 1994 and June–October 1996	see Newcomer et al. [2000]; Bubier et al. [1995, 2000]

[a]Shemya United States Air Force (USAF) Base station.
[b]National Oceanic and Atmospheric Administration (NOAA).
[c]Canadian Atmospheric Environment Service (AES); Climate Research Unit (CRU) of the University of East Anglia in the United Kingdom (Mitchell et al., submitted manuscript, 2004).

between the simulated and observed maximum daily CH$_4$ consumption rate is minimized at these sites. Specifically, we alter the parameters of the methane module until the simulated CH$_4$ consumption by soils reaches the maximum consumption rate of 0.95, 1.2, and 2.7 mg CH$_4$ m^{-2} d^{-1} at the B-F, Tundra-NS, and Tundra-UI sites, respectively. Because the meteorological observations of some sites are not available to us, we use climatic data from other sources (see Table 2), and it is possible that this may lead to biases in the parameterization. In addition, our approach of adjusting a single parameter at a time may lead to biases in parameterizations. The ecosystem-specific parameters for the MDM based on these site calibrations are documented in Table 1.

2.3. Model Testing at the Site Level

[24] To test the model and validate our parameterizations, we conduct simulations for a boreal forested wetland site (NSA-FEN) in Canada and a tundra site (Tundra-F) at Fairbanks, Alaska (Table 2), which are not used during our parameterization process. To evaluate model performance, we compare the simulated daily CH$_4$ fluxes to observed fluxes at these sites. The SSA-FEN parameterization is used for the NSA-FEN site simulations, and the Toolik-W parameterization is used for the Tundra-F site simulations.

2.4. Regional Simulations Using Geographically Explicit Data

[25] To make spatially and temporally explicit estimates of CH$_4$ emissions and consumption in the northern high latitudes (north of 45°N) with our new version of TEM, we use spatially explicit data of climate, land cover, soils, daily climate, and monthly leaf area index (LAI) from a variety of sources. The model is applied at the spatial resolution of 0.5° latitude × 0.5° longitude and at a daily time step for the period 1900 through 2000.

[26] The static data sets include potential vegetation [Melillo et al., 1993], soil texture [Zhuang et al., 2003], the distribution of wet soils and the fractional inundation of wetlands [Matthews and Fung, 1987], and soil-water pH [Carter and Scholes, 2000]. Similar to earlier versions of TEM, the vegetation and soil texture data sets are used to assign vegetation-specific and texture-specific parameters to a grid cell. The remaining spatially explicit data sets are needed to provide inputs into the new MDM. The wet soils and the fractional inundation of wetlands data sets are used to derive the proportions of wetlands and uplands within each 0.5° × 0.5° grid cell. The soil-water pH data set is used to estimate methanogenesis across the study region.

[27] The daily climate data sets are derived from the historical monthly air temperature, precipitation, vapor pressure, and cloudiness data sets (T. D. Mitchell et al., A comprehensive set of high-resolution grids of monthly climate for Europe and the globe: The observed record (1901–2000) and 16 scenarios (2001–2100), submitted to Journal of Climatology, 2004) (hereinafter referred to as Mitchell et al., submitted manuscript, 2004) of the Climatic Research Unit (CRU) of the University of East Anglia in the United Kingdom. We linearly interpolate the monthly air temperature and vapor pressure to daily data using three

consecutive month's data. To determine a current month's daily air temperatures, for example, we assume that (1) the value of day 15 is equal to the current month's mean air temperature, (2) the value of the first day is equal to the average monthly air temperature of the current month and the previous month, and (3) the value of last day is equal to the average monthly air temperature of the current and the next month. The temperatures for the other days are linearly interpolated using values of the first, fifteenth, and last days. To convert monthly precipitation into daily rainfall, we use the statistical algorithm of *Li and Frolking* [1992] and *Liu* [1996]. The algorithm converts the monthly precipitation into a number of rainfall events of different duration and intensity based on air temperature and the correlation of monthly precipitation with the frequency of heavy, intermediate, and small rainfall events.

[28] In the HM, monthly LAI is used to estimate transpiration (Appendix D) [*Zhuang et al.*, 2002]. We use monthly LAI data sets derived from satellite imagery for the period 1982 to 1999 [*Myneni et al.*, 1997, 2001] to prescribe LAI for each 0.5° latitude × 0.5° longitude grid cell. From 1900 to 1981, we use the LAI of 1982 to represent LAI during this period. We also use the LAI of 1999 to represent LAI during 2000. During our simulations, LAI is assumed to remain constant within a month.

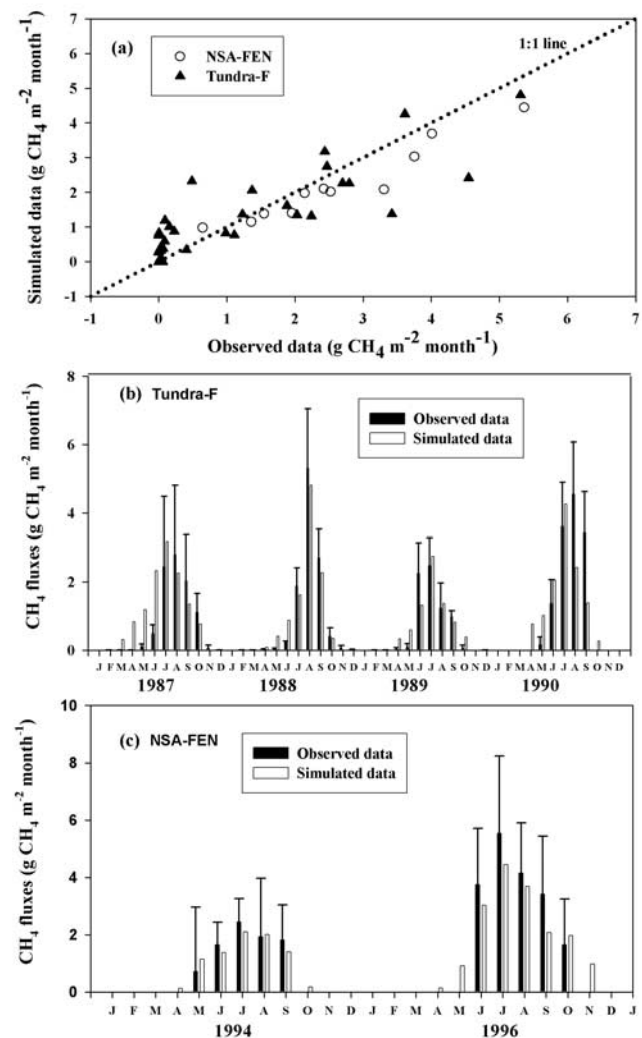[29] To develop regional estimates of CH_4 exchange from 1900 to 2000, we simulate the methane dynamics and estimate daily CH_4 fluxes from both wetland and upland ecosystems in each 0.5° latitude × 0.5° longitude grid cell. These ecosystem-specific CH_4 flux estimates are then area-weighted for each grid cell, as defined by the fractional inundation data set of *Matthews and Fung* [1987], to determine the CH_4 fluxes from each 0.5° latitude × 0.5° longitude grid cell.

3. Results and Discussion

3.1. Site-Specific Testing

[30] At the test site Tundra-F, the simulation captures the interannual and seasonal variations of the net CH_4 emissions. The simulated annual emissions are 12.2, 10.4, 7.6, and 12.1 g CH_4 m^2 yr^{-1} for 1987, 1988, 1989, and 1990, respectively, compared to observed emissions of 8.05 ± 2.5, 11.38 ± 2.88, 8.11 ± 1.80, and 13.64 ± 1.20 g CH_4 m^2 yr^{-1} for the same years [see *Whalen and Reeburgh*, 1992]. The geometric mean regression statistics [*Sokal and Rohlf*, 1981] shows a significant ($P < 0.01$; $N = 48$ months) relationship between the simulated and observed monthly emissions with $R^2 = 0.77$, slope = 0.86 ± 0.06, and intercept = 0.17 ± 0.10 g CH_4 m^{-2} $month^{-1}$ (Figure 2a). Overall, the

Figure 2. Comparisons between simulated and observed CH_4 emissions at the test sites including (a) a scatterplot of observed versus simulated monthly CH_4 emissions for the two sites; (b) a time series of the observed and simulated monthly CH_4 emissions at the Tundra-F site during the period 1987 to 1990; and (c) a time series of the simulated and observed monthly CH_4 emissions at the NSA-FEN test site during 1994 and 1996. The test sites are described in Table 2. The dashed line in Figure 2a indicates the 1:1 line for the regressions. For the NSA-FEN site, the statistics are significant ($P < 0.01$, $N = 10$ months) with $R^2 = 0.90$, slope = 0.70 ± 0.07, and intercept = 0.35 ± 0.23 g CH_4 m^{-2} $month^{-1}$. Similarly, for the Tundra-F site, the statistics are significant ($P < 0.01$, $N = 48$ months) with $R^2 = 0.77$, slope = 0.86 ± 0.06, and intercept = 0.17 ± 0.10 g CH_4 m^{-2} $month^{-1}$. Error bars in Figure 2b indicate the standard deviations for the mean monthly observations from three tussock tundra subsites, T1, T2, and T3; see *Whalen and Reeburgh* [1992] for more details. The observed monthly data in Figure 2b is aggregated from available daily data from February to December of 1987, January to December of 1988 and 1989, and from May to September of 1990. The observed daily data in Figure 2c are averaged from CH_4 chamber flux measurements at six subsites in 1994 and four subsites in 1996. These subsites represent the range of plant communities, water chemistry, and peatland types found in northern peatlands, including bog, rich fen, poor fen, and collapse scars. The observed monthly data in Figure 2c is aggregated from available daily data from May to September of 1994 and from June to October of 1996. Error bars in Figure 2c indicate the standard deviations for the mean monthly observations from these subsites.

simulations tend to have higher emissions compared to the observations during the spring of each year (Figure 2b). This discrepancy occurs because the model assumes that the winter snowpack insulates the soil from the frigid air temperatures during the winter such that soil temperatures remain relatively high. The higher soil temperatures lead to an earlier spring thaw, which in turn leads to earlier CH_4 production at the site. In 1990, the model underestimates the emissions in August and September. This is primarily because the simulated water table ranges from 27 to 28 cm, which is deeper than the measured maximum depth of 23 cm. The deeper water table leads to less CH_4 production and emissions.

[31] Similarly, at the NSA-FEN test site, the model is able to capture the interannual and seasonal dynamics of net CH_4 emissions in 1994 and 1996. A geometric mean regression between the monthly simulated and observed net emissions is significant ($P < 0.01$; $N = 10$ months) with $R^2 = 0.90$, slope = 0.73 ± 0.07, and intercept = 0.35 ± 0.23 g CH_4 m^{-2} $month^{-1}$ (Figure 2a). The model slightly underestimates the emissions from June to September in 1996 (Figure 2c). Our analyses suggest that the lower emissions in our simulation are primarily due to the lower soil temperatures resulting from the low soil thermal conductivity prescribed for the model at this site. The deviation is also partially due to the climate data used to drive the model. Owing to the lack of in situ meteorological data at the site, data from the Thompson station of the Canadian Atmospheric Environment Service (AES) has been used to drive the model for this analysis.

3.2. Contemporary Regional and Subregional Fluxes

[32] Overall, our simulations estimate that the Pan-Arctic region has been a mean source of about 51 T g CH_4 yr^{-1} during the 1990s. This estimate is in the same range as a number of other recent estimates that have been made using a variety of approaches (Table 3). Differences between our estimates and those of other studies may be a result of using different geographical boundaries or assuming different importance of various ecosystems in contributing methane to the atmosphere. For example, *Walter et al.* [2001b] considered areas north of 30°N in developing their regional estimates rather than the 45°N boundary used in this study. Several studies considered only tundra, boreal forests, or wetlands when developing their regional estimates. In our study, we estimate that the source strength varies over the Pan-Arctic and that large regions have actually been small net sinks of atmospheric CH_4 (Figure 3).

[33] In our simulations, wetlands act as a net source of CH_4, whereas upland areas act as a net sink. We estimate that wetlands across the Pan-Arctic emitted about 57 T g CH_4 yr^{-1} during the 1990s. Wetlands within boreal forests have the highest rates of emissions (23 g CH_4 m^{-2} yr^{-1}), but the large areas of wetlands within wet tundra cause these ecosystems to be the largest contributor of atmospheric CH_4.

[34] In addition to the estimates of net CH_4 emissions from wetlands, our simulations estimate that soil microbes in upland areas have consumed about 6 Tg CH_4 yr^{-1} across the Pan-Arctic during the 1990s. This estimate is higher in comparison to most other studies of methane consumption (Table 3), which estimate the consumption rate to be

Table 3. Emissions, Consumption, and Net Emissions of Methane From Ecosystem Soils Across the Pan-Arctic Region During the 1990s

	Emissions, Tg CH_4 yr^{-1}	Consumption, Tg CH_4 yr^{-1}	Net Emissions, Tg CH_4 yr^{-1}
TEM	57.3	6.3	51.0
Other studies			
Whalen and Reeburgh [1992]	42 ± 26[a]		
Whalen and Reeburgh [1990a]	53[b]		
Sebacher et al. [1986]	$45-106$[c]		
Bartlett and Harriss [1993]	38[d]		
Matthews and Fung [1987]	62[e]		
Crill et al. [1988]	72[f]		
Walter et al. [2001a]	65[g]		
Cao et al. [1998]	31[h]		
Harriss et al. [1993]	35[i]		
Liu [1996]	47[j]		
Born et al. [1990]		$1-15$[k]	
Whalen et al. [1991]		$0-0.8$[l]	
Steudler et al. [1989]		$0.3-5.1$[m]	
Ridgwell et al. [1999]		5.5[n]	
Potter et al. [1996]		2.4[o]	
Chen [2004]			$42-45$[p]

[a]Estimates for Arctic wet meadow and tussock and shrub tundra.
[b]Estimates for global tundra and taiga ecosystems.
[c]Estimates for Arctic and boreal wetlands.
[d]Estimates for northern wetlands north of 45°N.
[e]Estimates for forested and non-forested bogs between 50°N and 70°N.
[f]Estimates for undrained peatlands north of 40°N.
[g]Estimates for wetlands north of 30°N.
[h]Estimates for natural wetlands north of 40°N.
[i]Estimates for northern tundra and taiga.
[j]Estimates for natural wetlands between 40°N and 80°N.
[k]Estimates for boreal forests.
[l]Estimates for upland and floodplain taiga.
[m]Estimates for boreal forests.
[n]Estimates for tundra and boreal forests.
[o]Estimates for tundra and boreal forests.
[p]Estimates based on inverse modeling for the Northern Hemisphere.

between 0 and 5.5 Tg CH_4 yr^{-1}. An exception is the *Born et al.* [1990] study, which suggested a consumption rate of up to 15 Tg CH_4 yr^{-1}. In developing our estimates of CH_4 emissions, we do not consider the potential effects of moisture hindrance on methane diffusion through unsaturated soil. As a result, our model may overestimate actual consumption rates. Upland areas within wet tundra have the highest consumption rates (0.27 g CH_4 m^{-2} yr^{-1}) because the simulated soil moisture in wet tundra is closer to the optimum soil moisture for methanotrophy than that simulated for upland boreal forests.

[35] The simulated CH_4 emissions and consumption vary across the region as a result of the distribution of wetlands as well as the spatial variability in climate (Figure 3). For the 1990s, our simulations estimate that terrestrial ecosystems within Russia, Canada, and Alaska are the major sources of CH_4 emissions in the Pan-Arctic, which are contributing 64%, 11%, and 7%, respectively, of the total net CH_4 emissions per year (51.0 Tg CH_4 yr^{-1}, Table 4). Within Russia, we estimate that the net CH_4 emissions from the West Siberia wetlands are 21g CH_4 m^{-2} yr^{-1}, for a total of 12 Tg CH_4 yr^{-1}, which is close to the high end of the mean estimates of $0.3-14$ Tg CH_4 yr^{-1} by *Smith et al.* [2004], but lower than the mean estimate of 26 g CH_4
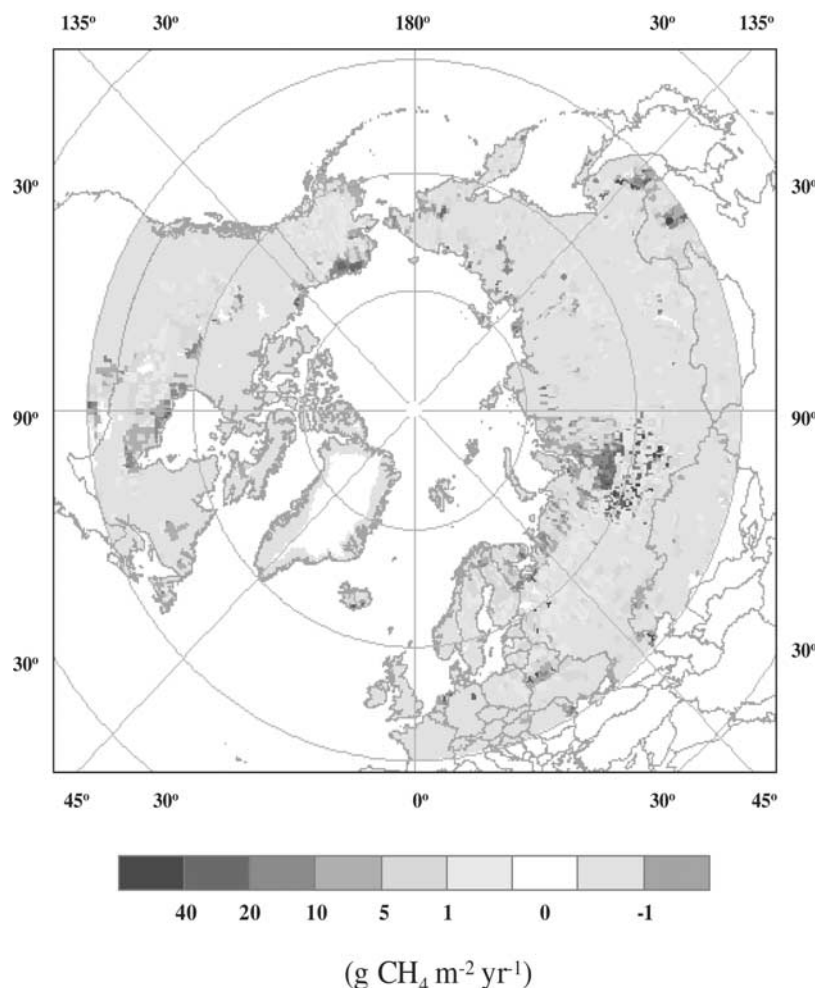
Figure 3. Simulated net CH_4 emissions and consumption in the Pan-Arctic region during the 1990s. Positive values indicate the net CH_4 release to the atmosphere, and negative values indicate the CH_4 uptake from the atmosphere. See color version of this figure at back of this issue.

m^{-2} yr^{-1} by *Friborg et al.* [2003] for this region. Consumption of methane is more evenly distributed across the Pan-Arctic. The soils of Russia, Canada, and Alaska account for 38%, 25%, and 5%, respectively, of the total CH_4 consumed per year (6.3 Tg CH_4 yr^{-1}, Table 4) in this region.

[36] Our simulations indicate that 60% of the net CH_4 emissions come from the latitude band of 45°N–60°N as compared to 40% of total emissions from the region of 60°N–75°N, Table 5). This pattern is probably due to the larger areas of wetlands in the southern Pan-Arctic compared to the middle Pan-Arctic. However, wetlands represent a

larger proportion of the land area in the middle Pan-Arctic than the southern Pan-Arctic such that the mean net emissions per square meter are actually higher in the middle Pan-Arctic. The consumption in the southern Pan-Arctic is also 2 times larger than in the middle Pan-Arctic, which is primarily due to the larger forest area in the southern Pan-Arctic.

Table 5. Latitudinal Variations in Emissions, Consumption, and Net Emissions of Methane During the 1990s

	Northern Pan-Arctic (75°N–90°N)	Middle Pan-Arctic (60°N–75°N)	Southern Pan-Arctic (45°N–60°N)	Pan-Arctic (45°N-90°N)
Emissions, Tg CH_4 yr^{-1}	0.2	23.0	34.0	57.3
Consumption, Tg CH_4 yr^{-1}	−0.2	−2.0	−4.0	−6.3
Net emissions, Tg CH_4 yr^{-1}	0.0	21.0	30.0	51.0
Land area, 10^{10} m^2	58.7	1473.3	2294.6	3826

Table 4. Regional Variation in Emissions, Consumption, and Net Emissions of Methane During the 1990s

	Russia	Canada	Alaska	Pan Arctic
Emissions, Tg CH_4 yr^{-1}	35.1	7.1	3.8	57.3
Consumption, Tg CH_4 yr^{-1}	−2.3	−1.5	−0.3	−6.3
Net emissions, Tg CH_4 yr^{-1}	32.8	5.6	3.5	51.0
Land area, 10^{10} m^2	687.4	370.2	65.2	3826

Table 6. Decadal Variations in Climate, Net Primary Productivity (NPP), and CH_4 Fluxes for the Past Century in the Pan-Arctic Region

	1900s	1910s	1920s	1930s	1940s	1950s	1960s	1970s	1980s	1990s
CH_4 emissions, Tg CH_4 yr^{-1}	47.8	48.0	51.5	51.7	50.7	53.4	50.7	50.7	53.8	57.3
CH_4 consumption, Tg CH_4 yr^{-1}	−6.0	−6.1	−6.1	−6.2	−6.2	−6.2	−6.1	−6.2	−6.2	−6.3
Net CH_4 emissions, Tg CH_4 yr^{-1}	41.8	41.9	45.4	45.5	44.5	47.2	44.6	44.5	47.6	51.0
Mean annual air temperatures, °C	−4.0	−4.0	−3.7	−3.5	−3.5	−3.7	−3.7	−3.7	−3.3	−2.9
Mean annual precipitation, mm	471	474	473	478	484	494	505	503	507	505
Mean annual soil temperatures, °C	−1.2	−1.2	−1.0	−0.9	−0.9	−1.0	−1.0	−1.0	−0.7	−0.5
Mean annual water table depths, mm	198.6	198.8	199.5	200.5	200.5	199.6	199.6	200.0	201.5	202.9
NPP, Pg C yr^{-1}	8.3	8.4	8.3	8.6	8.7	8.7	8.7	8.7	9.0	9.1

3.3. Twentieth Century Trends

[37] During the past century, our simulations estimate that net CH_4 emissions have increased at a rate of 0.08 Tg CH_4 yr^{-1} estimated as the slope of the linear regression between the annual net emissions and year from 1900 to 2000. For the 1980s, however, the model simulates a larger increasing trend in CH_4 emissions ($\sim$1.0 Tg CH_4 yr^{-1}, estimated as the slope of the linear regression between the annual net emissions and year from 1980 to 1989). The increased trend of net emissions during this period is consistent with the increased trend (11.6 ± 0.2 ppbv yr^{-1}) of the observed atmospheric CH_4 concentrations during 1983–1991 in the Northern Hemisphere [*Dlugokencky et al.*, 1994].

[38] While methane consumption rates remain fairly constant throughout the study period, net CH_4 emissions vary from decade to decade (Table 6) with relatively large emissions in the 1920s–1930s, 1950s, and 1980s–1990s. The decadal net CH_4 emission rates are correlated with decadal variations in climate and its derived variables, namely, soil temperature, water table depth, and NPP. Our analyses indicate that net CH_4 emissions are more significantly correlated with air temperature (R^2 = 0.81; P < 0.01, N = 10 decades) than precipitation (R^2 = 0.40; P < 0.01; N = 10 decades). The correlations between decadal net CH_4 emissions and water table depth, soil temperature, and NPP are significantly (P < 0.01) high, with R^2 values of 0.65, 0.82, and 0.65, respectively. These analyses suggest that changes in climate and its influence on ecosystem production and the soil environment could significantly influence the dynamics of CH_4 emissions.

[39] Decadal changes of simulated monthly emissions from the 1900s to 1990s also show an increasing trend in the magnitude of net CH_4 emissions during the growing season (May through September; see Figure 4) when root exudates provide additional carbon for methanogenesis. As shown in Table 6, NPP has increased over the period. The enhanced NPP increased the input of root exudates to enhance methanogenesis and CH_4 emissions over this time period. Our simulations show that the peak emissions occurred in July, which is consistent with the results of recent inverse modeling studies [*Houweling et al.*, 2000; *Chen*, 2004] and other process-based modeling [*Cao et al.*, 1996]. This peak in monthly CH_4 emissions corresponds to the seasonal peak in NPP.

[40] Our simulations also show that large interannual variability in net CH_4 emissions occurred during the twentieth century (Figures 5a and 5b). For example, our simulations estimate that the net CH_4 emissions decrease from

50 Tg CH_4 yr^{-1} in 1991 to 40 and 45 Tg CH_4 yr^{-1} in 1992 and 1993, respectively, after the Mount Pinatubo eruption in 1991 (Figure 5c). This pattern of CH_4 emissions has also been observed in the inverse modeling study of *Dlugokencky et al.* [1994], and the modeling study of *Walter et al.* [2001b]. During 1998, there was a large positive anomaly in the global growth rate of atmospheric methane concentrations; *Dlugokencky et al.* [2001] attributed this anomaly in part to increased emissions from wetlands in northern high latitudes resulting from warm conditions in 1998 due to the strong El Niño phenomena. Our simulation results support this interpretation and indicate that the
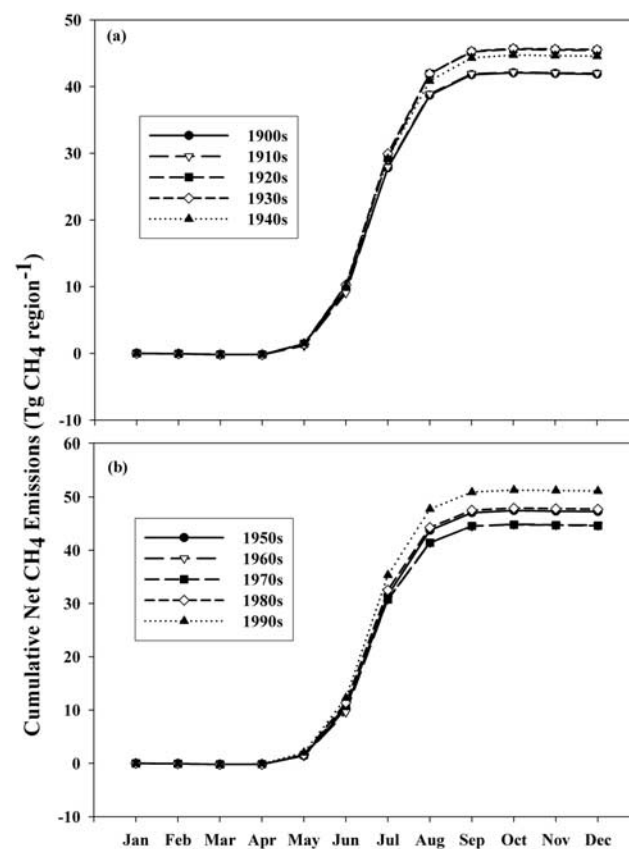

Figure 4. Cumulative net CH_4 emissions from the Pan-Arctic region for each decade from (a) the 1900s to the 1940s and (b) the 1950s to the 1990s. Net CH_4 emissions of each month are averaged over each decade.
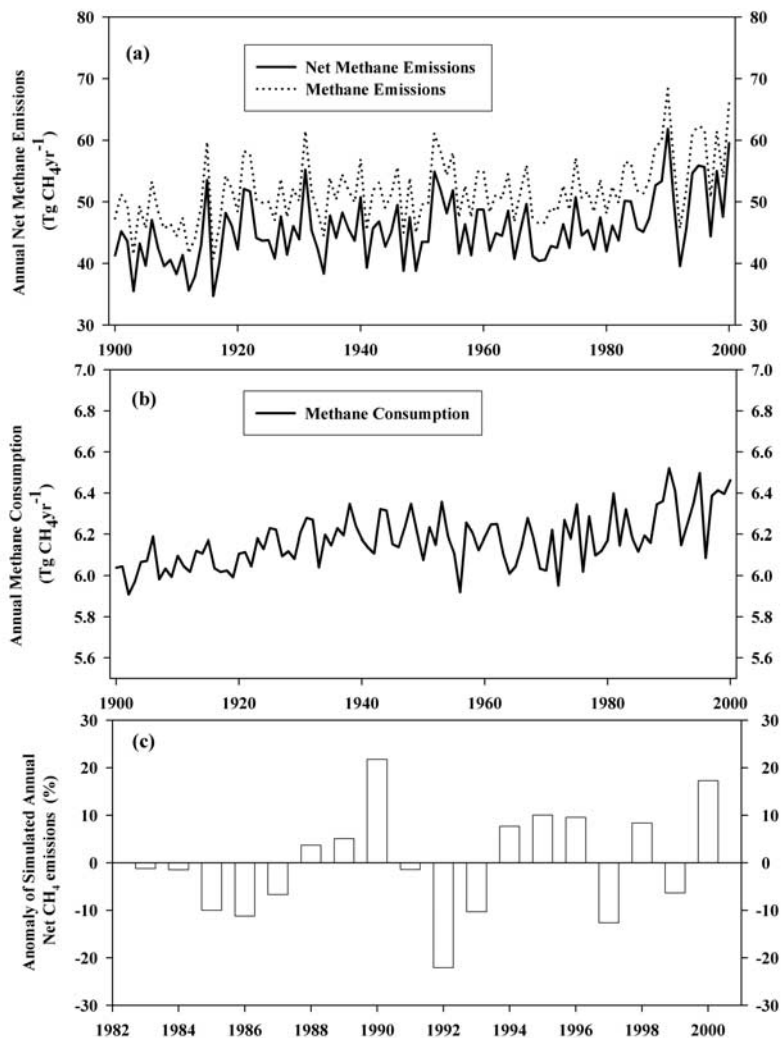
Figure 5. Annual methane fluxes from the Pan-Arctic region during the twentieth century including (a) annual net methane emissions, (b) annual methane consumption, and (c) anomaly of simulated net CH_4 emissions from 1983 to 2000. Anomalies are calculated based on the averaged net CH_4 emissions from 1982 to 2000.

region released 55 Tg CH_4 in 1998, an amount that is 8–11 Tg higher than the net CH_4 emissions in 1999 and 1997. However, we acknowledge that the atmospheric CH_4 concentrations are influenced by a variety of factors including atmospheric transport and atmospheric CH_4 oxidation as well as CH_4 emissions from other sources such as fires, landfills, industrial processing, fossil-fuel burning, and rice paddies. Thus net CH_4 emissions from natural wetlands can only partially explain the changes in atmospheric CH_4 concentrations and may at times show opposite trends. For example, our simulated net CH_4 emissions for the year 2000 are the second highest emissions estimated during the last decade or so in response to interannual climate variability, but the atmospheric CH_4 concentrations did not show a corresponding peak due to a number of different sink and source dynamics. A decrease in fire disturbances north

of 38°N [van der Werf et al., 2004] and their associated emissions during 2000 may have compensated for the increases in net CH_4 emissions from wetlands to influence atmospheric CH_4 concentrations.

3.4. Sensitivity of Net CH_4 Emissions to Active Layer Depth

[41] Previous studies [Zhuang et al., 2001; Romanovsky and Osterkamp, 1997] have indicated that the active layer depth may be significantly overestimated if soil thermal models do not consider the possibility of soil freezing upward from the permafrost boundary. Because the estimated active layer depth is used to determine the lower boundary of microbial activity including methanogenesis in soils of permafrost regions, the overprediction of the active layer depth will result in higher estimates of methane production and emissions. To test this hypothesis, we

increase the depth of the lower boundary by 10 cm in a sensitivity analysis. The resulting regional estimate of net CH_4 emissions for the Pan-Arctic region is 38% larger than that of our control simulations. This suggests that the consideration of two freezing fronts, i.e., freezing of soil upward from the permafrost boundary as well as downward from the soil surface, is important when modeling methane emissions from regions underlain with permafrost.

3.5. Conclusions

[42] In this study, we couple key aspects of soil thermal, hydrological, and carbon dynamics of terrestrial ecosystems with methane cycling to estimate CH_4 fluxes between the atmosphere and the soils of the Pan-Arctic region. By considering the ability of soils to produce methane in wetland soils and to oxidize methane in both wetland and upland soils, we have developed more comprehensive regional estimates of CH_4 fluxes than provided by earlier studies using either process-based models or field estimates. Our analyses suggest that CH_4 emissions are more sensitive to changes in climate, particularly air temperature, than consumption, such that natural ecosystems may become a larger source of atmospheric CH_4 with future global warming. In addition, our analyses suggest that changes in root exudates associated with climate-induced enhancements in plant productivity may also increase CH_4 emissions. However, reductions in the area of wetlands in the Pan-Arctic region [e.g., *McGuire et al.*, 2004] as a result of alterations of the hydrological cycle may decrease methane production and allow methane consumption by soils to become more important. Because the areal extent of wetlands has been kept constant in this study, we have not been able to evaluate the importance of this negative feedback on regional estimates of net CH_4 emissions.

[43] Our regional estimates of net CH_4 emissions from natural ecosystems are 10–20% higher than those estimated from an inverse modeling study based on spatial and temporal changes in atmospheric CH_4 concentrations [*Chen*, 2004]. To help resolve this discrepancy and to better understand the role of natural ecosystems in the global methane budget, it is desirable to couple our spatially explicit estimates of CH_4 fluxes to an atmospheric transport model to simulate seasonal and interannual changes in atmospheric CH_4 concentrations. This approach has already been taken with CO_2 fluxes and has proved helpful in evaluating and improving the simulation of the various aspects of the carbon cycle including terrestrial carbon sequestration [*McGuire et al.*, 2000; *Dargaville et al.*, 2002; *Zhuang et al.*, 2003].

Appendix A: Methane Production

[44] Methane (CH_4) production occurs in the saturated zone of soils. As described by equation (3) in the text, we simulate hourly CH_4 production rates as a function of carbon substrate availability, soil thermal conditions, soil pH, and soil redox potentials. The influence of carbon substrate availability on methanogenesis is documented in section 2.1.4. Here we describe, in more detail, the influ-

ence of soil thermal conditions, soil pH conditions, and soil redox potentials on the production rate of methane.

A1. Effects of Soil Temperatures on Methanogenesis

[45] Many studies indicate that soil temperature influences the rate methane production [e.g., *Bartlett and Harriss*, 1993; *Frolking and Crill*, 1994; *Christensen et al.*, 1995]. Here we assume the hourly methane production rate increases logarithmically with soil temperature based on work by *Walter and Heimann* [2000],

$$f(M_{ST}(z,t)) = P_{Q10}^{\frac{T_{SOIL}(z,t) - T_{PR}}{10}}, \tag{A1}$$

where P_{Q10} is an ecosystem-specific Q_{10} coefficient (Table 1); $T_{SOIL}(z, t)$ is the hourly soil temperature at depth z (centimeters) and time t (hours), which is simulated by the STM module for each 1 cm depth of the soil profile; and T_{PR} is the reference temperature for methanogenesis that varies across ecosystems (Table 1).

A2. Soil pH Effects on Methanogenesis

[46] The optimal soil-water pH for methanogenesis ranges from 6.4 to 7.8 [*Minami*, 1989; *Wang et al.*, 1993] with a tolerance that ranges from 5.5 to 9.0 [*Skinner*, 1968; *Wang et al.*, 1993]. If pH is above or below the tolerance range, methanogenesis is completely inhibited. Therefore, following *Cao et al.* [1996], we model the effect of soil pH on hourly methane production as

$$f(pH(z,t)) = \frac{(pH - pH_{MIN})(pH - pH_{MAX})}{(pH - pH_{MIN})(pH - pH_{MAX}) - (pH - pH_{OPT})^2}, \tag{A2}$$

where pH is the soil-water pH value at the site, pH_{MIN} is the minimum soil-water pH, pH_{MAX} is the maximum soil-water pH, and pH_{OPT} is the optimum soil-water pH for methane production. We assume values of 5.5, 9.0 and 7.5 for pH_{MIN}, pH_{MAX}, and pH_{OPT}, respectively, for all soils. We also assume that the pH prescribed for a site is the same at each soil depth z (centimeters) and time t (hours).

A3. Redox Potential Effects on Methanogenesis

[47] Redox potential (E_{HL}) is used to model the relative availability of electron acceptors (e.g., O_2, NO_3^-, SO_4^{-2}, Fe^{+3}, Mn^{+4}), which suppress methanogenesis [*Segers and Kengen*, 1998]. On the basis of work by *Zhang et al.* [2002] and *Fiedler and Sommer* [2000], the effects of daily redox potential on hourly CH_4 production is modeled for each 1 cm depth as follows:

$$f(R_x(z,t)) = 1.0 \qquad E_{HL}(z,u) \leq -200 \text{ mV}, \tag{A3a}$$

$$f(R_x(z,t)) = \alpha \times E_{HL}(z,u) - 1.0$$
$$-100 \text{ mV} > E_{HL}(z,u) > -200 \text{ mV}, \tag{A3b}$$

$$f(R_x(z,t)) = 0.0 \qquad E_{HL}(z,u) \geq -100 \text{ mV}, \tag{A3c}$$

where $E_{HL}(z, u)$ is the estimated daily redox potential (mV) at soil depth z and day u and α is a constant (-0.01 mV^{-1}).

[48] Following *Zhang et al.* [2002] and *Segers and Kengen* [1998], we model daily changes in E_{HL} as a function of the root distribution, the fraction of water filled pore space, and the water table position at the site,

$$\frac{dE_{HL}(z, u)}{du} = C_R \times (A_L - 1.0), \qquad (A4a)$$

if the depth z is in the saturated zone, or

$$\frac{dE_{HL}(z, u)}{du} = C_R \times (A_L + 1.0 - F_W(z)), \qquad (A4b)$$

if depth z is in the unsaturated zone, and

$$A_L = F_{CA} \times P_A \times R_{LD}, \qquad (A5)$$

where C_R is the change rate of soil redox potential under saturated conditions; $F_W(z)$ is the fraction of water-filled pore space at depth z; F_{CA} is the cross-sectional area of a typical fine root; P_A is a scalar for the degree of gas diffusion from root to atmosphere; and R_{LD} is the fine root length density. We assume that C_R is 100 mV, F_{CA} is 0.0013 m^2, and R_{LD} is 10 m m^{-3} [see *McClaugherty et al.*, 1982] for all ecosystems. We assume P_A is 0.0 for forested ecosystems and 0.5 for other ecosystems [*Zhang et al.*, 2002]. The HM determines $F_W(z)$ for each 1 cm depth based on soil moisture and the porosity of the corresponding HM soil layer (i.e., moss or litter, upper organic, lower organic, upper mineral, or lower mineral, [see *Zhuang et al.*, 2002]).

Appendix B: Methane Oxidation

[49] Methane oxidation occurs in upland soils and the unsaturated zone of wetland soils. The oxygenase pathway of methane oxidation dominates methanotrophy in terrestrial ecosystems. As described by equation (4) in the text, we model the oxidation rate as a function of soil CH$_4$ concentration, soil temperature, soil moisture, and soil redox potential. Below, we describe in more detail the influence of each factor used in this equation.

B1. Effects of CH$_4$ Concentrations on Methanotrophy

[50] Methane oxidation requires the methane substrate to be present in the soil. This substrate may be available in a soil layer either as a result of methanogenesis within that soil layer or by diffusion of methane into the soil layer from the surrounding soil layers or the atmosphere. Diffusion of methane through the soil profile is discussed in Appendix C. If the methane substrate is present, we assume that the effect of the CH$_4$ concentration on oxidation follows Michaelis-Menten kinetics [see *Bender and Conrad*, 1992],

$$f(C_M(z, t)) = \frac{C_M(z, t)}{K_{CH4} + C_M(z, t)}, \qquad (B1)$$

where $C_M(z, t)$ is the hourly soil CH$_4$ concentration (μmol L^{-1}) at depth z (centimeters) and time t (hours); and K_{CH4} is the ecosystem-specific half saturation constant for CH$_4$ concentrations (Table 1). Typical values of K_{CH4} constants range between 1 and 66.2 μmol L^{-1}.

B2. Effects of Soil Temperature on Methanotrophy

[51] Similar to methanogenesis, methanotrophy is influenced by soil temperatures. On the basis of *Walter and Heimann* [2000], we assume the hourly oxidation rate increases logarithmically with soil temperature,

$$f(T_{SOIL}(z, t)) = O_{Q10}^{\frac{T_{TSOIL}(z, t) - T_{OR}}{10}}, \qquad (B2)$$

where O_{Q10} is an ecosystem-specific Q_{10} coefficient (Table 1); $T_{SOIL}(z, t)$ is the hourly soil temperature at depth z (centimeters) and time t (hours), which is simulated by the STM module for each 1 cm depth of the soil; and T_{OR} is the reference soil temperature (°C) that varies with vegetation type (Table 1).

B3. Effects of Soil Moisture on Methanotrophy

[52] A variety of studies indicate that soil moisture is a predictor of methane oxidation rate [e.g., *Steudler et al.*, 1989; *Gulledge and Schimel*, 1998]. However, some recent modeling efforts have not considered the importance of this factor to methanotrophy [e.g., *Walter and Heimann*, 2000; *Zhang et al.*, 2002]. Here we assume that the effect of soil moisture on methane oxidation is similar to the effect of soil moisture on decomposition of soil organic carbon [see *Tian et al.*, 1999]. Therefore we model the influence of volumetric soil moisture on methanotrophic microbial activity as

$$f(E_{SM}(z, t)) = \frac{(M_V - M_{V\min})(M_V - M_{V\max})}{[(M_V - M_{V\min})(M_V - M_{V\max})] - (M_V - M_{Vopt})^2}, \qquad (B3)$$

where $M_{v\min}$, M_{vopt}, and $M_{v\max}$ are the minimum, optimum, and maximum volumetric soil moistures for the methanotrophic reaction, respectively, which vary among ecosystems (Table 1); M_V is the soil moisture at each 1 cm depth of the soil, which is estimated by the HM.

B4. Effects of Redox Potential on Methanotrophy

[53] Redox potential (E_{HL}) is used to model the relative availability of electron acceptors (e.g., O$_2$, NO$_3^-$, SO$_4^{-2}$, Fe^{+3}, Mn^{+4}) on methane oxidation. Oxygen in the soil is the primary electron acceptor for this process [*Segers*, 1998]. However, methane oxidation may still occur under anaerobic conditions (i.e., E_{HL} less than 300 mV), if alternative electron acceptors are available. To simulate these effects, we use the relationship between redox potential and methane oxidation described by *Zhang et al.* [2002],

$$f(R_{OX}(z, t)) = 0.0 \qquad E_{HL}(z, u) < -200 \text{ mV}, \qquad (B4)$$

$$f(R_{OX}(z, t)) = \beta \times E_{HL}(z, u) + 1.5$$
$$-100 \text{ mV} \geq E_{HL}(z, u) \geq -200 \text{ mV}, \qquad (B5)$$

$$f(R_{OX}(z, t)) = \gamma \times E_{HL}(z, u) + \frac{5}{6}$$
$$200 \text{ mV} \geq E_{HL}(z, u) > -100 \text{ mV}, \qquad (B6)$$

$$f(R_{OX}(z, t)) = 1.0 \qquad E_{HL}(z, u) > 200 \text{ mV}, \qquad (B7)$$

where $f(R_{OX}(z, t))$ is the effect of redox potential at depth z (centimeters) and time t (hours); $E_{HL}(z, u)$ is the estimated daily redox potential at depth z and day u; and β and γ are constants, which equal 0.0075 mV^{-1} and 8.3 $\times$ 10^{-4} mV^{-1}, respectively. The calculation of daily changes in $E_{HL}(z, u)$ is described in section A3 of Appendix A.

Appendix C: Methane Transport

[54] The atmosphere, vegetation, and soils are treated as a continuum for the movement of methane from soils to the atmosphere. Transport of methane from soils to the atmosphere can occur via three different pathways: diffusion, plant-aided emissions, and ebullition. In upland soils, we assume that diffusion of atmospheric methane into soils is the sole method of moving methane through the soil. However, in wetland soils, we assume that all three pathways are important. Here we describe, in more detail, how we estimate the transport of methane through these pathways and how they influence our estimates of methane fluxes between the soil and the atmosphere.

C1. Methane Diffusion

[55] We assume that diffusion of methane occurs throughout the soil profile based on the concentration gradient of methane within the soil following Fick's law through coarse soil pores,

$$F_D(z, t) = -D(z)\frac{\partial C_M(z, t)}{\partial z}, \tag{C1}$$

where $F_D(z, t)$ is the diffusive flux at depth z (centimeters) and time t (hours), and $C_M(z, t)$ is the corresponding methane concentration (μmol L^{-1}). The diffusion coefficient, $D(z)$ in units of cm^{-2} h^{-1}, is modeled as

$$D(z) = 0.66 \times D_i \times f(\text{coarse}), \tag{C2}$$

where 0.66 is the tortuousity coefficient, suggesting that the distance covered by diffusion is about two thirds of the length of the real average path; D_i is the molecular diffusion coefficient of methane, which is 0.2 cm^2 s^{-1} in unsaturated soil layers and 0.00002 cm^2 s^{-1} in saturated soil layers [*Walter and Heimann*, 2000]; and $f(\text{coarse})$ is the relative volume of the coarse pores. The difference in D_i between the unsaturated and saturated soil layers reflects the difference in the rate of molecular diffusion of methane through air versus water; we do not consider potential effects of soil moisture on hindrance diffusion under saturated conditions. In addition to tortuousity and soil moisture, the diffusion of methane through soil depends on soil porosity [*Dörr et al.*, 1993], which is a function of soil texture. To account for the influence of porosity, the factor $f(\text{coarse})$ is calculated as

$$f(\text{coarse}) = \text{SAND} \times \text{PV}_{\text{SAND}} + \text{SILT} \times \text{PV}_{\text{SILT}}$$
$$+ \text{CLAY} \times \text{PV}_{\text{CLAY}}, \tag{C3}$$

where SAND, SILT, and CLAY represent the relative contents of sand, silt, and clay (%) in the soil, which are prescribed for a site; and PV$_{\text{SAND}}$, PV$_{\text{SILT}}$, and PV$_{\text{CLAY}}$

denote the relative volume of coarse pores in sandy, silty, and clayish soils, respectively. These latter parameters are set to 0.45, 0.20, and 0.14, respectively, following *Walter et al.* [2001a]. The $F_D(z, t)$ for each 1 cm depth can be deduced simultaneously from equation (C1) and equation (1) using the Crank-Nicolson method [*Press et al.*, 1990]. For boundary conditions, the CH$_4$ concentration change at the lower boundary (L_B) is set to zero and the CH$_4$ concentration at the soil surface (or water surface if the water table is at or above the soil surface) is set to 0.076 μmol L^{-1} to represent the atmospheric CH$_4$ concentration. Diffusion from only the surface soil layer contributes to methane emissions to the atmosphere or to the consumption of atmospheric methane by soils as $F_D(z = 0, t)$.

C2. Plant-Aided Transport

[56] The root systems of some plants also provide a more direct conduit for methane produced at depth in the soil to reach the atmosphere. As described by *Walter and Heimann* [2000], the rate at which methane is removed from a soil layer at depth z (centimeters) and time t (hours) through vegetation roots, $R_P(z, t)$ is modeled as a function of the quality of plant-mediated transport at a site (TR$_{\text{VEG}}$), the distribution of roots in the soil, the growth stage of vegetation during the growing season, and the distribution of soil methane concentrations ($C_M(z, t)$) in the soil,

$$R_P(z, t) = K_P \text{TR}_{\text{VEG}} f_{\text{ROOT}}(z) f_{\text{GROW}}(t) C_M(z, t), \tag{C4}$$

where K_P is a rate constant of 0.01 h^{-1}; $f_{\text{ROOT}}(z)$ is a multiplier that describes the effects of the relative amount of root biomass at depth z (centimeters); and $f_{\text{GROW}}(t)$ is a multiplier that describes the effect of growth stage at time t (hours). The term TR$_{\text{VEG}}$ depends on vegetation type and plant density. Because we assume that trees do not contribute to plant-aided transport, we set TR$_{\text{VEG}}$ equal to 0.0 for boreal forests. As grasses and sedges, which are similar to tussock tundra, are good gas transporters [*Walter*, 1998] and shrubs are very poor gas transporters [*Walter and Heimann*, 2000], we set TR$_{\text{VEG}}$ equal to 0.5 for tundra ecosystems that we consider to be a mosaic of tussock and shrub tundra. The density of roots is assumed to decrease linearly with depth. Thus the $f_{\text{ROOT}}(z)$ multiplier is determined as follows:

$$f_{\text{ROOT}}(z) = 2 \times \left(1 - \frac{z}{R_D}\right) \qquad z \leq R_D \tag{C5a}$$

$$f_{\text{ROOT}}(z) = 0.0 \qquad z > R_D, \tag{C5b}$$

where R_D is the rooting depth (centimeters), which is determined from vegetation type and soil texture [*Vörösmarty et al.*, 1989]. Similar to *Walter and Heimann* [2000], we also assume that the ability of plants to conduct methane varies with the life history of the plant, with the maximum conductance of methane occurring in mature plants. To simulate the effect of growth stage on $R_P(z, t)$, we calculate $f_{\text{GROW}}(t)$ based on an assumed relationship

between leaf area index (LAI) and soil temperatures(T_{S20}) described by *Walter and Heimann*, [2000],

$$f_{\text{GROW}}(t) = \text{LAI}_{\min} \qquad T_{S20} < T_{gr}, \qquad (\text{C6a})$$

$$f_{\text{GROW}}(t) = \text{LAI}_{\min} + \text{LAI}_{\max}\left(1 - \left(\frac{T_{mat} - T_{S20}}{T_{mat} - T_{gr}}\right)^2\right) \qquad (\text{C6b})$$
$$T_{gr} \le T_{S20} \le T_{mat},$$

$$f_{\text{GROW}}(t) = \text{LAI}_{\max} \qquad T_{mat} < T_{S20}, \qquad (\text{C6c})$$

where $\text{LAI}_{\min}$ is the minimum LAI associated with the beginning of plant growth; $\text{LAI}_{\max}$ is the maximum LAI associated with plants at maturity; T_{gr} is the temperature at which plants start to grow; and T_{mat} is the temperature at which plants reach maturity during the growing season. Similar to *Walter and Heimann* [2000], $\text{LAI}_{\min}$ and $\text{LAI}_{\max}$ have been chosen to be 0 and 4, respectively; T_{gr} is equal to 2°C where the annual mean soil temperature is below 5°C, and otherwise, T_{gr} is equal to 7°C; and T_{mat} is assumed to equal $T_{gr} + 10$°C. However, unlike *Walter and Heimann* [2000], we have chosen to use the mean soil temperature across the top 20 cm of the soil profile to represent T_{S20} rather than the temperature at the 50 cm depth. Our previous studies [*Zhuang et al.*, 2002, 2003] have demonstrated that using the mean soil temperature of the top 20 cm of the soil profile, which roughly represents the organic soil layer, is more useful for determining seasonal soil carbon and nitrogen dynamics.

[57] A few studies [e.g., *Schipper and Reddy*, 1996; *Gerard and Chanton*, 1993] have indicated that methane may be oxidized in the small oxic zone around root tips, although the proportion of methane that is oxidized by this pathway is highly uncertain. We assume that 40% of the methane in plant-mediated transport is oxidized before the gas reaches the atmosphere, which is less than the 50% oxidized assumed by *Walter and Heimann* [2000]. The methane emissions transported through the plant-mediated pathway to the atmosphere is obtained integrating $R_p(z, t)$ over the soil profile from the rooting depth to the soil surface as

$$F_P(t) = \int_{R_D}^{0} R_p(z,t)\,dz. \qquad (\text{C7})$$

C3.   Methane Ebullition

[58] The formation of bubbles in the soil profile allows methane to be transported through the soil more rapidly than would be predicted by diffusion alone. Following *Walter and Heimann* [2000], the loss of methane through bubbles ($R_E(z, t)$) from a soil layer at depth z (centimeters) and time t (hours) is modeled as a function of soil CH_4 concentrations $f(C_M(z, t))$,

$$R_E(z,t) = K_e f(C_M(z,t)), \qquad (\text{C8a})$$

if z is below the water table, and

$$R_E(z,t) = 0.0, \qquad (\text{C8b})$$

if z is above the water table. K_e is a rate constant of 1.0 h^{-1}. If the methane concentration $C_M(z, t)$ is greater than a threshold for bubble formation (M_{TH}), $f(CM(z, t))$ is equal to the difference between $CM(z, t)$ and M_{TH}; otherwise, $f(CM(z, t))$ is equal to 0.0. A value of 500 μmol L^{-1} is assumed to represent M_{TH} [*Walter and Heimann*, 2000] for all the ecosystems in our study. From the soil layers below the water table depth, bubbles are assumed to reach the water table within 1 hour. If the water table is at or above the soil surface, ebullition is assumed to contribute to methane emissions to the atmosphere as $F_E(t)$, which is obtained by integrating $R_E(z, t)$ over the whole water saturated zone,

$$F_E(t) = \int_{L_B}^{W_T} R_E(z,t)\,dz, \qquad (\text{C9a})$$

if W_T is at or above the soil surface, and

$$F_E(t) = 0.0, \qquad (\text{C9b})$$

if W_T is below the soil surface, where W_T is the depth of the water table (centimeters); and L_B is the lower boundary of the soil (centimeters). If the water table is below the soil surface, the methane in bubbles is added to the methane concentration in the soil layer just above the water table. This methane then continues to diffuse upward through the soil profile. In this case, $F_E(t)$ equals 0.0.

Appendix D: Updated Hydrological Module

[59] The hydrological module (HM) [*Zhuang et al.*, 2002] has been revised to be appropriate for both upland and wetland soils. The revisions include improvements in the simulation of infiltration (I_F), evapotranspiration of the vegetation canopy (E_V), soil surface evaporation (E_S), snowmelt (S_{melt}), and sublimation (S_S) from the snowpack. In addition, soil moisture dynamics are represented in greater detail for upland soils, and algorithms, based on work by *Granberg et al.* [1999], have been added to simulate water content and water table depth in wetland soils.

D1.   Infiltration From the Soil Surface Into the Soil (I_F)

[60] The liquid water from rain throughfall or snowmelt either infiltrates into the soil column or is lost as surface runoff. In the work of *Zhuang et al.* [2002], all liquid water reaching the soil surface has been assumed to infiltrate into the soil column. In this study, we add algorithms to estimate surface runoff and subtract this estimate from rain throughfall and snowmelt to estimate infiltration (I_F). Following *Bonan* [1996], surface runoff is calculated using the Dunne runoff if the soil surface is saturated or the Horton runoff if the soil surface is not saturated. In the Dunne approach, all the water inputs at the surface (i.e., rain throughfall and snowmelt) are lost as

runoff because the soil is already saturated. In the Horton approach, runoff occurs even when the soil is not saturated, but the total water inputs at the surface are greater than the infiltration capacity, which depends on the water content of the surface soil layer relative to the saturated water content of this layer.

D2. Evapotranspiration From the Vegetation Canopy (E_V)

[61] In *Zhuang et al.* [2002], we simulated evapotranspiration by simulating transpiration and evaporation from the canopy with separate algorithms. In the updated HM, we have replaced these algorithms with those of *McNaughton and Jarvis* [1983], which are based on the Penman-Monteith approach. Evapotranspiration from the vegetation canopy (E_V) is estimated based on short-wave solar radiation absorbed by the vegetation canopy, air temperature, vapor pressure deficit, and canopy conductance. The amount of solar radiation absorbed by the canopy is determined using the incident short-wave solar radiation occurring at the top of the canopy and the leaf area index (LAI) of the vegetation [*Zhuang et al.*, 2002].

[62] Following *Rosenberg et al.* [1983], vapor pressure deficit is modeled as

$$\text{VPD} = 10 \times (E_{\text{adt}} - V_P), \qquad \text{(D1)}$$

where V_P is vapor pressure (kPa) from input data sets. E_{adt} is saturation vapor pressure (kPa),

$$E_{\text{adt}} = 0.61078 \times e^{\frac{17.269 \times T_A}{T_A + 237.3}}, \qquad \text{(D2)}$$

where T_A is air temperature (°C).

[63] A simplified equation of *Waring and Running* [1998] has been adopted to model the canopy water conductance (G),

$$G = g_{\max} f(T_A) f(\text{VPD}) f(\psi), \qquad \text{(D3)}$$

where $g_{\max}$ is the maximum canopy conductance (mm s^{-1}); $f(T_A)$ is a multiplier that describes the effect of air temperature (T_A) on the canopy conductance; $f(\text{VPD})$ is a multiplier that describes the effect of the vapor pressure deficit (VPD in mbar) on canopy conductance; and $f(\psi)$ is a multiplier that describes the effect of leaf water potential (lwp in MPa) on canopy conductance. We set $g_{\max}$ to be 3.5, 13.5, and 21.2 mm s^{-1} for alpine tundra, wet tundra, and boreal forests, respectively. The effects of air temperature on canopy conductance are calculated following *Thornton* [2000],

$$f(T_A) = 0.0 \qquad\qquad T_A < -8.0°C, \qquad \text{(D4a)}$$

$$f(T_A) = 1.0 + \eta \times T_A \qquad -8.0° < T_A < 0.0°C, \qquad \text{(D4b)}$$

$$f(T_A) = 1.0 \qquad\qquad T_A > 0.0°C, \qquad \text{(D4c)}$$

where η is a constant (0.125 °C^{-1}). The effects of vapor pressure deficit on canopy conductance are calculated as

$$f(\text{VPD}) = 0.0 \qquad\qquad \text{VPD} > \text{VPD}_{\text{close}}, \qquad \text{(D5a)}$$

$$f(\text{VPD}) = \frac{\text{VPD}_{\text{close}} - \text{VPD}}{\text{VPD}_{\text{close}} - \text{VPD}_{\text{open}}} \qquad \text{VPD}_{\text{open}} < \text{VPD} < \text{VPD}_{\text{close}}, \qquad \text{(D5b)}$$

$$f(\text{VPD}) = 1.0 \qquad \text{VPD} < \text{VPD}_{\text{open}}, \qquad \text{(D5c)}$$

where $\text{VPD}_{\text{close}}$ is the vapor pressure deficit at complete conductance reduction and VPD_{open} is the vapor pressure deficit at the start of canopy conductance reduction. We assume $\text{VPD}_{\text{close}}$ is 41.0 mbar and VPD_{open} is 9.3 mbar for all vegetation types.

[64] The effects of leaf water potential (lwp) on canopy conductance are calculated in a similar manner,

$$f(\psi) = 0.0 \qquad\qquad \text{lwp} < \psi_{\text{close}}, \qquad \text{(D6a)}$$

$$f(\psi) = \frac{\psi_{\text{close}} - \text{lwp}}{\psi_{\text{close}} - \psi_{\text{open}}} \qquad \psi_{\text{close}} < \text{lwp} < \psi_{\text{open}}, \qquad \text{(D6b)}$$

$$f(\psi) = 1.0 \qquad\qquad \text{lwp} > \psi_{\text{open}}, \qquad \text{(D6c)}$$

where ψ_{close} is the leaf water potential at complete conductance reduction and ψ_{open} is the leaf water potential at the start of conductance reduction. We assume that ψ_{close} is −2.3 MPa and ψ_{open} is −0.6 MPa for all vegetation types. As in the work of *Zhuang et al.* [2002], lwp is calculated as

$$\text{lwp} = \frac{0.2}{W_S / \text{SOIL}_{\text{CAP}}}, \qquad \text{(D7)}$$

where W_S is mean daily soil water content (millimeters) integrated across the soil profile from the upper boundary to the lower boundary, and SOIL_{CAP} is a parameter for soil water capacity (millimeters) of the soils, which is set to 235 [see *Zhuang et al.*, 2002].

D3. Evaporation From the Soil Surface (E_S)

[65] The evaporation rate from the soil surface is modeled using the Penman approach [*Zhuang et al.*, 2002], which uses air temperature, vapor pressure deficit, short-wave solar radiation at the soil surface, and the throughfall of rain from the overlying vegetation canopy. In the work of *Zhuang et al.* [2002], a mean daily rate of potential evaporation is estimated for a month and a monthly rate is determined by multiplying this mean daily rate by the number of days per month (M_D). In this study, we use the daily potential evaporation (PE$_S$) estimates directly (i.e., $M_D = 1.0$) when calculating daily evaporation from the soil surface (E_S). If the daily throughfall of rain (R_{TH}) is greater

than or equal to PE$_S$, then E_S is assumed to equal PE$_S$; otherwise, E_S is equal to R_{TH}.

D4. Snowmelt (S_{melt}) and Snow Sublimation (S_S)

[66] The rate of snowmelt has been modeled by *Zhuang et al.* [2002], using monthly shortwave solar radiation, throughfall of snow from the overlying vegetation canopy, snow albedo, and the number of days per month. The potential snowmelt rate (PS$_{melt}$ in millimeters) now uses a daily time step, which depends on daily air temperature and solar radiation [*Brubaker et al.*, 1996; Edward Rastetter, personal communication, 2002],

$$PS_{melt} = m_q \times \left(\frac{R_n/100.0}{0.2388} \right) + A_R \times T_A, \qquad (D8)$$

where m_q is a constant (2.99 kg MJ^{-1}), R_n is the incident short-wave solar radiation to the snowpack (J cm^{-2} d^{-1}), A_R is a constant (2.0 mm °C^{-1} d^{-1}), and T_A is the daily air temperature (°C). If the daily throughfall of snow is greater than PS$_{melt}$, then S$_{melt}$ is equal to PS$_{melt}$; otherwise S$_{melt}$ is equal to the daily throughfall of snow.

[67] The rate of snow sublimation has also been modeled by *Zhuang et al.* [2002] based on monthly short-wave solar radiation and throughfall of snow from the overlying vegetation canopy. In the work of *Zhuang et al.* [2002], a mean potential sublimation rate is determined and multiplied by the number of days per month (M_D) to obtain a monthly rate. In this study, we use the potential daily sublimation rate (PS$_S$) directly (i.e., M_D = 1.0) based on daily shortwave solar radiation. If the PS$_S$ is greater than water equivalent of the snowpack, then S_S is assumed to equal the water equivalent of the snowpack; otherwise S_S is assumed to equal PS$_S$.

D5. Upland Soils

[68] In the work of *Zhuang et al.* [2002], the soil profile has been represented with three soil layers: a moss or litter layer, an organic soil layer, and a mineral soil layer. Changes to the water content of the whole soil profile (W_S in millimeters) have depended on infiltration (I_F), evapotranspiration from the vegetation canopy (E_V), evaporation from the soil surface (E_S), and drainage from the deep mineral layer (D_R),

$$\frac{dW_S}{dt} = I_F - E_V - E_S - D_R. \qquad (D9)$$

Within each soil layer, changes in water content have been determined using a water balance approach similar to that described in equation (D9). The terms I_F and D_R are replaced by percolation into and out of a soil layer, respectively, and E_S is assumed to occur only from the top moss or litter layer. Only the organic soil and mineral soil layers are assumed to contribute to E_V, and this flux has been partitioned between the two layers based upon the relative soil water content of the two layers. Soil moisture has been assumed to be uniformly distributed within each of the three soil layers.

[69] To improve our simulation of water dynamics in upland soils in high-latitude ecosystems, we now repre-

sent the soil profile with six layers with different hydrologic characteristics: a 10-cm-thick moss or litter layer, a 20-cm-thick upper organic soil layer, a 40-cm-thick lower organic soil layer, an 80-cm-thick upper mineral soil layer, a 160-cm-thick lower mineral soil layer, and a 320-cm-thick deep mineral soil layer. We assume that all upland soils have the same soil profile structure for our soil water dynamics due to a lack of spatially explicit data sets for each grid cell. Changes to the water content of the entire soil profile are still influenced by the factors given in equation (D9). However, soil moistures within each of the six layers are now assumed to vary as described by the Richards equation [*Hillel*, 1980; *Celia et al.*, 1990],

$$\frac{\partial W_C}{\partial t} = \frac{\partial}{\partial z} \left(k \left(\frac{\partial W_C}{\partial z} \frac{\partial \psi_S}{\partial W_C} + 1 \right) \right), \qquad (D10)$$

where W_C is the volumetric water content (mm^3 mm^{-3}); k is the hydraulic conductivity (mm s^{-1}); and ψ_s is the soil matrix potential (millimeters), which varies as a function of W_C and soil texture [*Clapp and Hornberger*, 1978]. The soil water content (W_C) for the midpoint of each of the different layers of the unsaturated soils is obtained simultaneously through solving equations (D9) and (D10) numerically with a tridiagonal system of equations [see *Press et al.*, 1990]. Infiltration (I_F) into the first soil layer sets the upper boundary condition for the numerical solution and the drainage (D_R) of the deep mineral soil layer, which is equal to the hydraulic conductivity of this layer, sets the lower boundary condition. Although the Richards equation could be used to estimate soil moistures at each 1 cm depth in the profile, large amounts of computation time would be required to extrapolate this approach across the Pan-Arctic. Instead, we use the soil moisture contents at the midpoints of each of the six soil layers to interpolate soil moistures at each 1 cm depth across the soil profile.

D6. Wetland Soils

[70] Because *Zhuang et al.* [2002] only considered water dynamics in unsaturated soils, new algorithms needed to be developed to estimate the proportion of the soil profile that becomes saturated, the depth of the resulting water table, and the influence of the water table on soil moisture in the unsaturated portion of the soil profile. We assume that wetland soils are always saturated below 30 cm, which represents the maximum water table depth (z_b). Thus changes in water content (W_S) of the top 30 cm of the soil profile can be calculated with a water balance model that considers the water input and outputs at the daily time step,

$$\frac{dW_S}{dt} = I_F - E_V - E_S - Q_{DR}, \qquad (D11)$$

where I_F is infiltration, E_V is evapotranspiration of the vegetation canopy, E_S is evaporation from the soil surface, and Q_{DR} is the saturated flow drainage below z_b. Calculation of the I_F, E_V, and E_S terms for wetlands use the same algorithms that have been described in the

previous sections of Appendix D. Similar to *Walter et al.* [2001a], Q_{DR} is calculated as

$$Q_{DR} = Q_{DRMAX} \times f(\text{coarse}), \tag{D12}$$

where Q_{DRMAX} is the maximum drainage rate of 20 mm d^{-1}; and f(coarse) is the relative volume of coarse pores in the soil. The calculation of f(coarse) is described in equation (C3).

[71] Instead of the six layers used to simulate upland soils, we assume that water dynamics in wetland soils can be represented by two functional layers or "zones": an upper oxygenated, unsaturated zone; and a lower anoxic, saturated zone. The water table represents the boundary between these two zones, and its depth is allowed to change over time with changes in soil moisture. The maximum thickness of the upper unsaturated layer is represented by the maximum water table depth (z_b), which is assumed to be 30 cm [*Frolking et al.*, 1996; *Granberg et al.*, 1999]. The minimum thickness of the lower saturated layer is the difference between the depth of the lower boundary (L_B) and 30 cm. The total volume of water in the top 30 cm of the soil profile (V_{TOT} in centimeters) is represented by

$$V_{TOT} = \phi(z_b - W_T) + \int_{W_T}^{0} \theta_{us}(z)dz, \tag{D13}$$

where ϕ is the soil porosity, W_T is the actual water table depth (centimeters), and $\theta_{us}(z)$ is the volumetric water content in the unsaturated zone at depth z. We assume ϕ is equal to 0.9 cm^3 cm^{-3} [*Frolking and Crill*, 1994] for the entire soil profile. If W_S is greater than $z_b \times \phi$, the water table will be above the soil surface and the height of water above the soil surface is determined by the difference of W_S and $z_b \times \phi$. Otherwise, V_{TOT} is equal to W_S. After setting V_{TOT} to equal W_S, equation (D13) can be integrated and inverted to solve for the water table depth (W_T) following *Granberg et al.* [1999],

$$W_T = \sqrt{\frac{3(\phi \times z_b - W_W)}{2a_z}} \quad z \leq z_{\theta s,\min} \tag{D14a}$$

$$W_T = \frac{3(\phi \times z_b - W_W)}{2(\phi - \theta_{s,\min})} \quad z > z_{\theta s,\min}, \tag{D14b}$$

where a_z is the gradient in soil moisture resulting from evaporation at the soil surface and is calculated as the ratio of ϕ-$\theta_{s,\min}$ to $z_{\theta s,\min}$; $\theta_{s,\min}$ is the minimum volumetric water content at the soil surface; and $z_{\theta s,\min}$ is the maximum depth where evaporation influences soil moisture. We assume $\theta_{s,\min}$ is 0.25 and $z_{\theta s,\min}$ is 10 cm for all wetland soils. A negative value of the water table depth indicates that the water table is above the soil surface, whereas a positive value indicates that the water table is below the soil surface.

[72] After determining the water table depth, the volumetric water content at each 1 cm depth can then be estimated. If depth z is in the saturated zone, the volumetric water content is assumed to be equal to ϕ. If depth z is in the unsaturated zone, the volumetric water content ($\theta_{us}(z)$) is estimated following *Granberg et al.* [1999],

$$\theta_{us}(z) = \min\left(\phi, \theta_s + (\phi - \theta_s)\left(\frac{z}{W_T}\right)^2\right), \tag{D15}$$

where θ_s is the volumetric water content at the soil surface and is calculated as

$$\theta_s = \max(\theta_{s,\min}, \phi - (a_z \times W_T)). \tag{D16}$$

Notation

ϕ	soil porosity in wetlands (cm^3 cm^{-3}).
α, η, β, and γ	constants as -0.01 mV^{-1}, 0.125 °C^{-1}, 0.0075 mV^{-1}, 8.3×10^{-4} mV^{-1}, respectively.
ψ_{close}, ψ_{open}	leaf water potential at complete conductance reduction (MPa), leaf water potential at the start of conductance reduction (MPa).
ψ_S	soil matrix potential (mm).
θ_s	volumetric water content at the soil surface (cm^3 cm^{-3}).
$\theta_{s,\min}$	minimum volumetric water content of the soil surface (cm^3 cm^{-3}).
$\theta_{us}(z)$	volumetric water content in the unsaturated zone at depth z (cm^3 cm^{-3}).
A_L	plant aerenchyma factor.
A_R	constant for calculating snowmelt (mm °C^{-1} d^{-1}).
a_z	gradient in soil moisture resulting from evaporation at the soil surface.
$C_M(z, t)$	soil CH$_4$ concentrations at depth z and time t (μmol L^{-1}).
C_R	change rate of soil redox potential under saturation conditions (100 mV).
$D(z)$	diffusion coefficient of methane (mol cm^{-2} h^{-1}).
D_i	molecular diffusion coefficient of methane in bulk air or in the saturated water soils (cm^2 s^{-1}).
D_R	drainage from the deep mineral layer in the upland soils (mm d^{-1}).
$E_{HL}(z, u)$	redox potential at soil depth z (mV) and day u.
E_V	evapotranspiration of the vegetation canopy (mm d^{-1}).
$f(\psi)$	multiplier that describes the effects of leaf water potential on canopy water conductance.

$f(C_{DIS}(z))$ multiplier that describes the relative availability of organic carbon substrate at depth z in the soils.

$f(C_M(z, t))$ multiplier that describes the effects of soil CH_4 concentrations on methanotrophy at depth z and time t.

$f(coarse)$ relative volume of the coarse pores in the soils (%).

$f(E_{SM}(z, t))$ multiplier that describes the effects of soil moisture on methanotrophy at depth z and time t.

$f(M_{ST}(z, t))$ multiplier that describes the effects of soil temperature on methanogenesis at depth z and time t.

$f(pH(t))$ multiplier that describes the effects of soil water pH on methanogenesis at time t.

$f(R_{OX}(z, t))$ multiplier that describes the effects of soil redox potentials on methanotrophy at depth z and time t.

$f(R_X(z, t))$ multiplier that describes the effects of redox potentials on methanogenesis at depth z and time t.

$f(S_{OM}(t))$ multiplier that describes the effects of methanogenic substrate availability on methanogenesis at time t.

$f(T_A)$ multiplier that describes the effects of air temperature on canopy water conductance.

$f(T_{SOIL}(z, t))$ multiplier that describes the effects of soil temperature on methanotrophy at depth z and time t.

$f(VPD)$ multiplier that describes the effects of the vapor pressure deficit on canopy water conductance.

F_{CA} cross-section area of a typical fine root (m^2).

$F_{CH4}(t)$ total flux of methane at the soil/water-atmosphere boundary via the different transport pathways at time t ($\mu mol\ h^{-1}$).

$F_D(z, t)$ diffusive flux of CH_4 through the soil layer at depth z and time t ($\mu mol\ h^{-1}$).

$F_D(z = 0, t)$ diffusive flux at the interface between the soil surface and the atmosphere at time t ($\mu mol\ h^{-1}$).

$F_E(t)$ ebullitive CH_4 emissions at time t ($\mu mol\ h^{-1}$).

$f_{GROW}(t)$ multiplier that describes the effects of the growing stage of vegetation on plant-aided CH_4 transport.

$F_P(t)$ plant-aided CH_4 emissions at time t ($\mu mol\ h^{-1}$).

$f_{ROOT}(z)$ multiplier that describes the effects of the vertical distribution of roots in the soils at depth z on plant-aided CH_4 transport.

$F_W(z)$ fraction of water filled pore space ($mm^3\ mm^{-3}$).

G canopy water conductance ($mm\ s^{-1}$).

g_{max} maximum canopy water conductance ($mm\ s^{-1}$).

I_F water infiltration ($mm\ d^{-1}$).

K hydraulic conductivity of the soils ($mm\ s^{-1}$).

K_{CH4} ecosystem-specific half saturation constant used in Michaelis-Menten kinetics of methane oxidation process ($\mu mol\ L^{-1}$).

K_e rate constant for CH_4 ebullitive transport (h^{-1}).

K_p rate constant for plant-aided CH_4 transport (h^{-1}).

LAI_{min}, LAI_{max} constants used for calculating the growing state of the plants ($m^2\ m^{-2}$).

L_B lower boundary of the modeled soil profile (cm).

L_{MAXB} prescribed maximum lower boundary (cm).

lwp leaf water potential (MPa).

M_D number of days within a month.

M_{GO} ecosystem-specific maximum potential CH_4 production rate ($\mu mol\ L^{-1}\ h^{-1}$).

$M_O(z, t)$ soil CH_4 oxidation rate at depth z and time t ($\mu mol\ L^{-1}\ h^{-1}$).

$M_P(z, t)$ soil CH_4 production rate at depth z and time t ($\mu mol\ L^{-1}\ h^{-1}$).

m_q constant used for calculating snow sublimation from the snowpack (2.99 $kg\ MJ^{-1}$).

M_{TH} threshold concentration for bubble formation ($\mu mol\ L^{-1}$).

$M_{vmax}, M_{vmin}, and\ M_{vopt}$ Maximum, minimum, and optimum volumetric soil moisture for methanotrophy ($mm^3\ mm^{-3}$).

$NPP(mon)$ monthly net primary productivity ($g\ C\ m^{-2}\ month^{-1}$).

NPP_{MAX} maximum monthly net primary productivity (NPP) for a particular ecosystem ($g\ C\ m^{-2}\ month^{-1}$).

O_{MAX} ecosystem-specific maximum oxidation coefficient (μmol L^{-1} h^{-1}).

O_{Q10} ecosystem-specific Q_{10} coefficient indicating the soil temperature dependency of methanotrophy.

P_A scalar used to indicate the degree of gas diffusion from plant roots to the atmosphere in plant-aided CH_4 transport.

pH_{MIN}, pH_{MAX}, pH_{OPT} minimum, maximum, and optimum soil pH, respectively for methanogenesis.

P_{Q10} ecosystem-specific Q_{10} coefficient indicating the dependency of CH_4 production to soil temperature.

PV_{SAND}, PV_{SILT}, PV_{CLAY} relative volumes of coarse pores in sandy, silty, and clayish soils, respectively (mm^3 mm^{-3}).

Q_{DR} saturated flow drainage below the maximum water table depth (mm d^{-1}).

Q_{DRMAX} maximum drainage rate below the maximum water table depth (mm d^{-1}).

R_D rooting depth (cm).

$R_E(z, t)$ soil CH_4 ebullitive emissions rate at depth z and time t (μmol L^{-1} h^{-1}).

R_{LD} fine root length density (m root m^{-3} soil).

R_n incident shortwave solar radiation at the top of the canopy (J cm^{-2} d^{-1}).

$R_P(z, t)$ plant-aided CH_4 emissions rate at depth z and time t (μmol L^{-1} h^{-1}).

SAND, SILT, and CLAY   relative contents of sand, silt, and clay, respectively, in soil(%).

S_{melt} snowmelt rate (mm d^{-1}).

$SOIL_{CAP}$ water capacity of the soils (mm).

S_S rate of sublimation from the snowpack (mm d^{-1}).

T_A daily air temperature (°C).

T_{gr} temperature at which plants start to grow (°C).

T_{mat} temperature at which plants reach maturity (°C).

T_{OR} ecosystem-specific reference soil temperature used in the Q_{10} function for simulating the effects of soil temperature on methanotrophy (°C).

T_{PR} ecosystem-specific reference temperature used in the Q_{10} function for simulating the effects of soil temperature on methanogenesis (°C).

TR_{VEG} multiplier that describes the effect of vegetation type and plant density on plant-aided CH_4 transport.

T_{S20} soil temperature across the top 20 cm of the soils (°C).

$T_{SOIL}(z, t)$ soil temperature at depth z and time t (°C).

V_P vapor pressure (kPa).

VPD   vapor pressure deficit (mbar).

VPD_{close}, VPD_{open} vapor pressure deficit at complete conductance reduction (mbar) and vapor pressure deficit at the start of canopy conductance reduction (mbar).

V_{TOT} total amount of water in the top 30 cm of the soil profile in wetlands (cm).

W_C volumetric water content (mm^3 mm^{-3}).

W_S mean daily soil water content integrated across the soil profile from the upper boundary to the lower boundary (mm).

W_T water table depth (cm).

$z_{\theta,min}$ maximum depth where evaporation influences soil moisture (cm).

z_b maximum water table depth (cm).

References

Bartlett, K. B., and R. C. Harriss (1993), Review and assessment of methane emissions from wetlands, *Chemosphere*, 26(1–4), 261–320.

Bender, M., and R. Conrad (1992), Kinetics of CH_4 oxidation in oxic soils exposed to ambient air or high CH_4 mixing ratios, *FEMS Microbiol. Ecol.*, 101, 261–270.

Bonan, G. B. (1996), Sensitivity of a GCM simulation to subgrid infiltration and surface runoff, *Clim. Dyn.*, 12, 279–285.

Born, M., H. Dörr, and I. Levin (1990), Methane concentration in aerated soils in West Germany, *Tellus, Ser. B*, 42, 58–64.

Brubaker, K., A. Rango, and W. Kustas (1996), Incorporate radiation inputs into the snowmelt runoff model, *Hydrol. Proc.*, 10, 1329–1343.

Bubier, J. L., T. R. Moore, L. Bellisario, N. T. Comer, and P. M. Crill (1995), Ecological controls on methane emissions from a northern peatland complex in the zone of discontinuous permafrost, Manitoba, Canada, *Global Biogeochem. Cycles*, 9(4), 455–470.

Bubier, J. L., P. M. Crill, and T. R. Moore (2000), Magnitude and control of trace gas exchange in boreal ecosystems, in *Collected Data of the Boreal Ecosystem-Atmosphere Study* [CD-ROM], edited by J. Newcomer et al., NASA Goddard Space Flight Cent., Greenbelt, Md.

Cao, M., S. Marshall, and K. Gregson (1996), Global carbon exchange and methane emissions from natural wetlands: Application of a process-based model, *J. Geophys. Res.*, 101(D9), 14,399–14,414.

Cao, M., K. Gregson, and S. Marshall (1998), Global methane emission from wetlands and its sensitivity to climate change, *Atmos. Environ.*, 32(19), 3293–3299.

Carter, A. J., and R. J. Scholes (2000), Soil data v2.0: Generating a global database of soil properties, report, Environ. CSIR, Pretoria.

Celia, M. A., E. T. Bouloutas, and R. L. Zarba (1990), A general mass-conservative numerical solution for the unsaturated flow equation, *Water Resour. Res.*, *26*(7), 1483–1496.

Chen, Y. (2004), Estimation of methane and carbon dioxide surface fluxes using a 3-D global atmospheric chemical transport model, Ph.D. thesis, Mass. Inst. of Technol., Cambridge, 180 pp.

Christensen, T. R., S. Jonasson, T. V. Callagham, and M. Havström (1995), Spatial variation in high-latitude methane flux along a transect across Siberian and European tundra environments, *J. Geophys. Res.*, *100*(D10), 21,035–21,045.

Clapp, R. B., and G. M. Hornberger (1978), Empirical equations for some soil hydraulic properties, *Water Resour. Res.*, *14*(4), 601–604.

Crill, P. M., K. B. Bartlett, R. C. Harriss, E. Gorham, E. S. Verry, D. I. Sebacher, L. Mazdar, and W. Sanner (1988), Methane flux from Minnesota peatlands, *Global Biogeochem. Cycles*, *2*(4), 371–384.

Dargaville, R. J., et al. (2002), Evaluation of terrestrial carbon cycle models with atmospheric CO_2 measurements: Results from transient simulations considering increasing CO_2, climate and land-use effects, *Global Biogeochem. Cycles*, *16*(4), 1092, doi:10.1029/2001GB001426.

Dise, N. B. (1993), Methane emission from Minnesota peatlands: Spatial and seasonal variability, *Global Biogeochem. Cycles*, *7*(1), 123–142.

Dlugokencky, E. J., K. A. Masaire, P. M. Lang, P. P. Tans, L. P. Steele, and E. G. Nisbet (1994), A dramatic decrease in the growth rate of atmospheric methane in the Northern Hemisphere during 1992, *Geophys. Res. Lett.*, *21*(1), 45–48.

Dlugokencky, E. J., B. P. Walter, K. A. Masarie, P. M. Lang, and E. S. Kasischke (2001), Measurements of an anomalous global methane increase during 1998, *Geophys. Res. Lett.*, *28*(3), 499–502.

Dörr, H., L. Katruff, and I. Levin (1993), Soil texture parameterization of the methane uptake in aerated soils, *Chemosphere*, *26*, 697–713.

Fiedler, S., and M. Sommer (2000), Methane emissions, groundwater levels and redox potentials of common wetland soils in a temperate-humid climate, *Global Biogeochem. Cycles*, *14*(4), 1081–1093.

Friborg, T., T. R. Christensen, and H. Soegaard (1997), Rapid response of greenhouse gas emission to early spring thaw in a subarctic mire as shown by micrometeorological techniques, *Geophys. Res. Lett.*, *24*(23), 3061–3064.

Friborg, T., H. Soegaard, T. R. Christensen, C. R. Lloyd, and N. S. Panikov (2003), Siberian wetlands: Where a sink is a source, *Geophys. Res. Lett.*, *30*(21), 2129, doi:10.1029/2003GL017797.

Frolking, S., and P. Crill (1994), Climate controls on temporal variability of methane flux from a poor fen in southeastern New Hampshire: Measurement and modeling, *Global Biogeochem. Cycles*, *8*(4), 385–397.

Frolking, S., et al. (1996), Modeling temporal variability in the carbon balance of a spruce/moss boreal forest, *Global Change Biol.*, *2*, 343–366.

Gerard, G., and J. Chanton (1993), Quantification of methane oxidation in the rhizosphere of emergent aquatic macrophytes: Defining upper limits, *Biogeochemistry*, *23*, 79–97.

Goodrich, L. E. (1978a), Some results of a numerical study of ground thermal regimes, paper presented at 3rd International Conference on Permafrost, Natl. Res. Counc. of Can., Ottawa.

Goodrich, L. E. (1978b), Efficient numerical technique for one-dimensional thermal problems with phase change, *Int. J. Heat Mass Transfer*, *21*, 615–621.

Granberg, G., H. Grip, M. O. Lofvenius, I. Sundh, B. H. Svensson, and M. Nilsson (1999), A simple model for simulation of water content, soil frost, and soil temperatures in boreal mixed mires, *Water Resour. Res.*, *35*(12), 3771–3782.

Gulledge, J., and J. P. Schimel (1998), Moisture control over atmospheric CH_4 consumption and CO_2 production in diverse Alaskan soils, *Soil Biol. Biochem.*, *30*(8/9), 1127–1132.

Harriss, R., K. Bartlett, S. Frolking, and P. Crill (1993), Methane emissions from northern high-latitude wetlands, *Biogeochemistry of Global Change: Radiatively Active Trace Gases*, edited by R. S. Oremland, pp. 449–486, Chapman and Hall, New York.

Hillel, D. (1980), *Fundamental of Soil Physics*, 413 pp., Academic, San Diego, Calif.

Houweling, S., F. Dentener, J. Lelieveld, B. Walter, and E. Dlugokencky (2000), The modeling of tropospheric methane: How well can point measurements be reproduced by a global model?, *J. Geophys. Res.*, *105*(D7), 8981–9002.

King, J., W. Reeburgh, and S. Regli (1998), Methane Flux Data, Alaska North Slope, 1994–1996, report, Natl. Snow and Ice Data Cent., Boulder, Colo. (Available at http://nsidc.org/data/arcss013.html)

King, S. L., P. D. Quay, and J. M. Lansdown (1989), The $^{13}C/^{12}C$ kinetic isotope effect for soil oxidation of methane at ambient atmospheric concentrations, *J. Geophys. Res.*, *94*(D15), 18,273–18,277.

Li, C., and S. Frolking (1992), Simulation of N_2O emission from soil by DNDC model with generalized climate scenarios, report, Univ. of N. H., Durham.

Liston, G. E., and R. A. Pielke (2000), A climate version of the regional atmospheric modeling system, *Theor. Appl. Climatol.*, *66*, 29–47.

Liu, Y. (1996), Modeling the emissions of nitrous oxide (N_2O) and methane (CH_4) from the terrestrial biosphere to the atmosphere, Ph.D. thesis, Mass. Inst. of Technol., 219 pp., Cambridge.

Matthews, E., and I. Fung (1987), Methane emissions from natural wetlands: Global distribution, area, and environmental characteristics of sources, *Global Biogeochem. Cycles*, *1*(1), 61–86.

McClaugherty, C. A., J. D. Aber, and J. M. Melillo (1982), The role of fine roots in the organic matter and nitrogen budgets of two forested ecosystems, *Ecology*, *63*(5), 1481–1490.

McGuire, A. D., J. M. Melillo, J. T. Randerson, W. J. Parton, M. Heimann, R. A. Meier, J. S. Clein, D. W. Kicklighter, and W. Sauf (2000), Modeling the effects of snowpack on heterotrophic respiration across northern temperate and high latitude regions: comparison with measurements of atmospheric carbon dioxide at high latitudes, *Biogeochemistry*, *48*, 91–114.

McGuire, A. D., et al. (2004), Canada and Alaska, in *Land Change Science: Observing, Monitoring, and Understanding Trajectories of Change on the Earth's Surface*, chap. 9, Kluwer Acad., Norwell, Mass., in press.

McNaughton, K. G., and P. G. Jarvis (1983), Predicting effects of vegetation changes on transpiration and evaporation, in *Water Deficits and Plant Growth*, vol. 7, pp. 1–47, Academic, San Diego, Calif.

Melillo, J. M., A. D. McGuire, D. W. Kicklighter, B. Moore III, C. J. Vörösmarty, and A. L. Schloss (1993), Global climate change and terrestrial net primary production, *Nature*, *63*, 234–240.

Minami, K. (1989), *Effects of Agricultural Management on Methane Emission From Rice Paddies*, Natl. Inst. of Agro-Environ. Sci., Tsukuba, Japan.

Moore, T. R., N. Roulet, and R. Knowles (1990), Spatial and temporal variations of methane flux from subarctic/northern boreal fens, *Global Biogeochem. Cycles*, *4*(1), 26–49.

Myneni, R. B., C. D. Keeling, C. J. Tucker, G. Asrar, and R. R. Nemani (1997), Increased plant growth in the northern high latitudes from 1981–1991, *Nature*, *386*, 698–701.

Myneni, R. B., J. Dong, C. J. Tucker, R. K. Kaufmann, P. E. Kauppi, J. Liski, L. Zhou, V. Alexeyev, and M. K. Hughes (2001), A large carbon sink in the woody biomass of northern forests, *Proc. Natl. Acad. Sci. USA.*, *98*(26), 14,784–14,789.

Newcomer, J., et al. (Eds.) (2000), *Collected Data of The Boreal Ecosystem-Atmosphere Study* [CD-ROM], NASA Goddard Space Flight Cent., Greenbelt, Md.

Ojima, D., A. Mosier, S. J. DelGrosso, and W. J. Parton (2000), TRAGNET analysis and synthesis of trace gas fluxes, *Global Biogeochem. Cycles*, *14*(4), 995–997.

Potter, C. S., E. A. Davidson, and L. V. Verchot (1996), Estimation of global biogeochemical controls and seasonality in soil methane consumption, *Chemosphere*, *32*, 2219–2246.

Prather, M., et al. (2001), Atmospheric chemistry and greenhouse gases, in *Climate Change 2001: The Scientific Basis—Contribution of Working Group I to the Third Assessment Report of the Intergovernmental Panel on Climate Change*, edited by J. T. Houghton et al., pp. 239–287, Cambridge Univ. Press, New York.

Press, W. H., B. P. Flannery, S. A. Teukolsky, and W. T. Vetterling (1990), *Numerical Recipes in C: The Art of Scientific Computing*, 735 pp., Cambridge Univ. Press, New York.

Prinn, R. G., et al. (1999), Integrated global system model for climate policy assessment: Feedbacks and sensitivity studies, *Clim. Change*, *41*(3/4), 469–546.

Ridgwell, A. J., S. J. Marshall, and K. Gregson (1999), Consumption of atmospheric methane by soils: A process-based model, *Global Biogeochem. Cycles*, *13*(1), 59–70.

Romanovsky, V. E., and T. E. Osterkamp (1997), Thawing of the active layer on the coastal plain of the Alaskan Arctic, *Permafrost Periglacial Proc.*, *8*, 1–22.

Romanovsky, V. E., T. E. Osterkamp, T. S. Sazonova, N. I. Shender, and V. T. Balobaev (2000), Past and future changes in permafrost temperatures along the East Siberian Transect and an Alaskan Transect, *Eos Trans. AGU*, *81*(48), Fall Meet. Suppl., Abstract B71F-09.

Rosenberg, N. J., B. L. Blad, and S. B. Verma (1983), *Microclimate: The Biological Environment*, second ed., pp. 1–495, John Wiley, Hoboken, N. J.

Schipper, L. A., and K. R. Reddy (1996), Determination of methane oxidation in the rhizosphere of *Sagittaria lancifolia* using methyl fluoride, *Soil Sci. Soc. Am. J.*, *60*, 611–616.

Sebacher, D. J., R. C. Harriss, K. B. Bartlett, S. M. Sebacher, and S. S. Grice (1986), Atmospheric methane sources: Alaskan tundra, an alpine fen and a subarctic boreal marsh, *Tellus, Ser. B.*, *38*, 1–10.

Segers, R. (1998), Methane production and methane consumption: A review of processes underlying wetland methane fluxes, *Biogeochemistry*, *41*, 23–51.

Segers, R., and S. W. M. Kengen (1998), Methane production as a function of anaerobic carbon mineralization: A process model, *Soil Biol. Biochem.*, *30*(8/9), 1107–1117.

Sellers, P. J., et al. (1997), BOREAS in 1997: Experiment overview, scientific results, and future directions, *J. Geophys. Res.*, *102*(D24), 28,731–28,769.

Skinner, F. A. (1968), *The Ecology of Soil Bacteria*, Univ. of Toronto Press, Toronto, Ont., Canada.

Smith, L. C., G. M. MacDonald, A. A. Velichko, D. W. Beilman, O. K. Borisova, K. E. Frey, K. V. Kremenetski, and Y. Sheng (2004), Siberian peatlands a net carbon sink and global methane source since the early Holocene, *Science*, *303*, 353–356.

Sokal, R. R., and F. J. Rohlf (1981), *Biometry: The Principles and Practice of Statistics in Biological Research*, 2nd ed., 859 pp., W. H. Freeman, New York.

Steudler, P. A., R. D. Bowden, J. M. Melillo, and J. D. Aber (1989), Influence of nitrogen fertilization on methane uptake in temperate forest soils, *Nature*, *341*, 314–316.

Suyker, A. E., S. B. Verma, R. J. Clement, and D. P. Billesbach (1996), Methane flux in a boreal fen: Season-long measurement by eddy correlation, *J. Geophys. Res.*, *101*(D22), 28,637–28,647.

Suyker, A. E., S. B. Verma, and T. J. Arkebauer (1997), Season-long measurement of carbon dioxide exchange in a boreal fen, *J. Geophys. Res.*, *102*(D24), 29,021–29,028.

Thornton, P. E. (2000), *Biome-BGC version 4.1.1*, report, Num. Terradyn. Simul. Group (NTSG), School of For., Univ. of Mont., Missoula.

Tian, H., J. M. Melillo, D. W. Kicklighter, A. D. McGuire, and J. Helfrich (1999), The sensitivity of terrestrial carbon storage to historical climate variability and atmospheric CO_2 in the United States, *Tellus, Ser. B*, *51*(2), 414–452.

van der Werf, G. R., J. T. Randerson, G. J. Collatz, L. Giglio, P. S. Kasibhatla, A. F. Arellano Jr., S. C. Olsen, and E. S. Kasischke (2004), Continental-scale partitioning of fire emissions during the 1997 to 2001 El Nino/La Nina period, *Science*, *303*, 73–76.

Vitt, H. D., L. A. Halsey, and S. C. Zoltai (2000), The changing landscape of Canada's western boreal forest: The current dynamics of permafrost, *Can. J. For. Res.*, *30*, 283–287.

Vörösmarty, C. J., B. Moore III, A. L. Grace, M. P. Gildea, J. M. Melillo, B. J. Peterson, E. B. Rastetter, and P. A. Steudler (1989), Continental scale models of water balance and fluvial transport: An application to South America, *Global Biogeochem. Cycles*, *3*(3), 241–265.

Walter, B. P. (1998), Development of a process-based model to drive methane emissions from natural wetlands for climate studies, dissertation, Max-Planck-Inst. für Meteorol., Hamburg, Germany.

Walter, B. P., and M. Heimann (2000), A process-based, climate-sensitive model to derive methane emission from natural wetlands: Application to five wetland sites, sensitivity to model parameters, and climate, *Global Biogeochem. Cycles*, *14*(3), 745–765.

Walter, B. P., M. Heimann, and E. Matthews (2001a), Modeling modern methane emissions from natural wetlands: 1. Model description and results, *J. Geophys. Res.*, *106*(D24), 34,189–34,206.

Walter, B. P., M. Heimann, and E. Matthews (2001b), Modeling modern methane emissions from natural wetlands: 2. Interannual variations 1982–1993, *J. Geophys. Res.*, *106*(D24), 34,207–34,219.

Wang, Z. P., R. D. Delaune, P. H. Masscheleyn, and W. H. Patrick Jr. (1993), Soil redox and pH effects on methane production in a flooded rice soil, *Soil Sci. Soc. Am. J.*, *57*, 386–391.

Waring, R. H., and S. W. Running (1998), *Forest Ecosystems, Analysis at Multiple Scales*, second ed., pp. 1–370, Academic Press, San Diego, Calif.

West, A. E., and S. K. Schmidt (1998), Wetting stimulates atmospheric CH_4 oxidation by alpine soil, *FEMS Microbiol. Ecol.*, *25*, 349–353.

Whalen, S. C., and W. S. Reeburgh (1990a), Consumption of atmospheric methane by tundra soils, *Nature*, *346*, 160–162.

Whalen, S. C., and W. S. Reeburgh (1990b), A methane flux transect along the trans-Alaska pipeline haul road, *Tellus, Ser. B*, *42*, 237–249.

Whalen, S. C., and W. S. Reeburgh (1992), Interannual variations in tundra methane emissions: A 4-year time series at fixed sites, *Global Biogeochem. Cycles*, *6*(2), 139–159.

Whalen, S., W. S. Reeburgh, and K. S. Kizer (1991), Methane consumption and emission by taiga, *Global Biogeochem. Cycles*, *5*(3), 261–273.

Zhang, Y., C. Li, C. C. Trettin, H. Li, and G. Sun (2002), An integrated model of soil hydrology, and vegetation for carbon dynamics in wetland ecosystems, *Global Biogeochem. Cycles*, *16*(4), 1061, doi:10.1029/2001GB001838.

Zhuang, Q., V. E. Romanovsky, and A. D. McGuire (2001), Incorporation of a permafrost model into a large-scale ecosystem model: Evaluation of temporal and spatial scaling issues in simulating soil thermal dynamics, *J. Geophys. Res.*, *106*(D24), 33,649–33,670.

Zhuang, Q., A. D. McGuire, K. P. O'Neill, J. W. Harden, V. E. Romanovsky, and J. Yarie (2002), Modeling the soil thermal and carbon dynamics of a fire chronosequence in interior Alaska, *J. Geophys. Res.*, *107*(D1), 8147, doi:10.1029/2001JD001244, 2002. [Printed *108* (D1), 2003].

Zhuang, Q., et al. (2003), Carbon cycling in extratropical terrestrial ecosystems of the Northern Hemisphere during the 20th century: A modeling analysis of the influences of soil thermal dynamics, *Tellus, Ser. B*, *55*, 751–776.

————————————

B. S. Felzer, S. Hu, D. W. Kicklighter, J. M. Melillo, P. A. Steudler, and Q. Zhuang, Ecosystems Center, Marine Biological Laboratory, 7 MBL Street, Woods Hole, 02543 MA, USA. (bfelzer@mbl.edu; shu@mbl.edu; dkick@mbl.edu; jmelillo@mbl.edu; steudler@mbl.edu; qzhuang@mbl.edu)

A. D. McGuire, U.S. Geological Survey, Alaska Cooperative Fish and Wildlife Research Unit, University of Alaska Fairbanks, Fairbanks, AK, USA. (ffadm@uaf.edu)

R. G. Prinn, Joint Program on the Science and Policy of Global Change, MIT E40-271, 77 Mass Ave, Cambridge, MA 02139, USA. (rprinn@mit.edu)
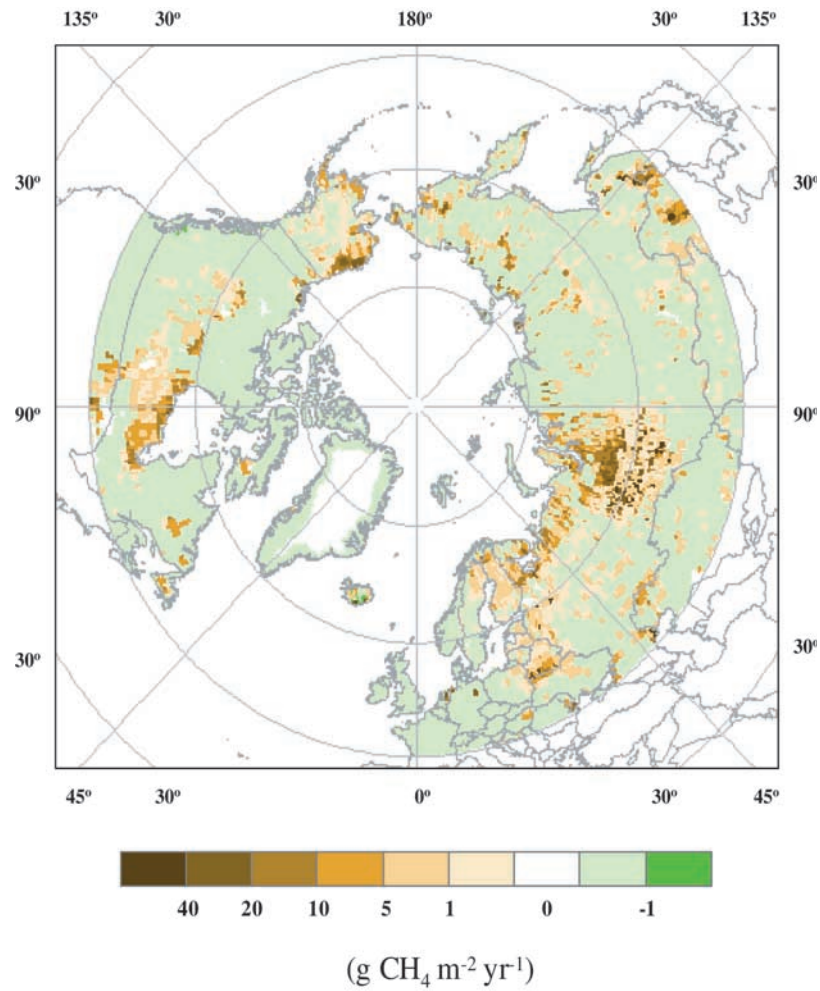
Figure 3. Simulated net CH_4 emissions and consumption in the Pan-Arctic region during the 1990s. Positive values indicate the net CH_4 release to the atmosphere, and negative values indicate the CH_4 uptake from the atmosphere.